

Supporting Information For:

Structure-property relationships for the force-triggered disrotatory ring-opening of cyclobutene

Brandon H. Bowser,[†] Cameron L. Brown,[†] Jan Meisner,^{‡,δ} Tatiana B. Kouznetsova,[†] Todd J. Martinez,^{*,‡,δ} and Stephen L. Craig^{*,†}

[†]Department of Chemistry, Duke University, Durham, NC, United States

[‡]Department of Chemistry, Stanford University, Stanford, CA, United States

*To whom correspondence should be addressed. Email: Todd.martinez@stanford.edu
stephen.craig@duke.edu

Table of Contents

Materials and Methods	2
General Information	2
Small Molecule Characterization	2
Details of SMFS Measurements	2
Synthetic Procedures	4
Modeling of Mechanophore-Embedded Polymer Extension	16
Modeling of Monomer Contour Lengths	17
Details of Constant-Velocity SMFS Analysis	26
Determination of Polymer Extension by Fitting to a FJC Model	26
Obtaining the plateau force value, f^*	27
Mechanical Activation by Pulsed Ultrasonication	32
FMPES Computations	38
NMR Spectra	42
References	62

Materials and Methods

General Information.

All reagents were purchased from Sigma-Aldrich, Alfa Aesar, or Tokyo Chemical Industry Co., LTD and used without further purification. Glassware was dried in an oven (160 °C) overnight and cooled under an inert gas (N₂ or Ar). All reactions were performed under nitrogen atmosphere. Flash chromatography was performed using Silicycle SiliaFlash® F60 gel (40-63 µm particle size, 230-400 mesh) and medium pressure liquid chromatography (MPLC) was performed on a Teledyne ISCO CombiFlash Rf 200. All gel permeation chromatography (GPC) was performed on in-line two columns (Agilent PLgel 10⁵ Å, 7.5 x 300 mm, 5µm, part number PL1110-6550) at room temperature using inhibitor free THF at a flow rate of 1.0 mL/min. The flow rate was set using an Agilent 1260 Infinity Isocratic pump, molecular weights were calculated using in line Wyatt Optilab T-rEX refractive index detector and Wyatt miniDAWN TREOS multi-angle light scattering detector, and UV absorbance was measured with an in-line Agilent 1260 Infinity UV detector. The UV detector monitored 190 to 800 nm with step of 2.0 nm and slit width of 4.0 nm. The refractive index increment (dn/dc) values were determined by using on-line 100% mass recovery assumption calculations built into Wyatt Astra software using injections of known concentration and mass. Before GPC analysis, 1-2 mg/mL in THF solutions were filtered through a 0.2 µm pore size PTFE syringe filters.

Small Molecule Characterization.

¹H-NMR and ¹³C-NMR spectra were obtained on either a 400 or 500 MHz Varian spectrophotometer and the residual solvent peaks (CDCl₃: 7.26 ppm [¹H], 77.16 ppm [¹³C]) were used as an internal chemical shift reference. All chemical shifts are given in ppm (δ) and coupling constants (J) in Hz as singlet (s), doublet (d), triplet (t), quartet (q), multiplet (m), or broad (b). High-resolution mass spectrometry was performed on an Agilent LCMS-TOF-DART at Duke University's Mass Spectrometry Facility.

Details of SMFS Measurements.

The AFM pulling experiments were conducted in toluene at an ambient temperature (~23 °C) in the same manner as described previously¹⁻⁵ using a homemade AFM, which was constructed using a Bruker (previously Digital Instruments) Multimode AFM head mounted on top of a piezoelectric positioner (Physik Instrumente, GmbH), similar to the one described in detail previously.⁶ Sharp Microlever silicon probes (MSNL) were purchased from Bruker (Camarillo, CA) and the force curves used for analysis were obtained with rectangular-shaped cantilevers (205 µm x 15 µm, nominal tip radius ~2 nm,

nominal spring constant $k \sim 0.02$ N/m, frequency ~ 15 kHz). Multiple probes of the same type were used throughout the course of the experiments. The spring constant of each cantilever was calibrated in air, using the thermal noise method, based on the energy equipartition theorem as described previously.⁷ Cantilever tips were prepared by soaking in piranha solution for ~ 15 min at room temperature. Silicon surfaces were prepared by soaking ~ 30 min in hot piranha solution, followed by washing with DI-water and drying under a stream of nitrogen. The surface and cantilever were then placed in a UVO cleaner (ozone produced through UV light) for 15 min. After ozonolysis, the cantilever was mounted, and ~ 20 μL of a ~ 0.1 - 0.05 mg mL^{-1} polymer solution was added to the silicon surface and allowed to dry. Measurements were carried out in a fluid cell with scanning set for a series of constant velocity approaching/retracting cycles. During acquisition data were filtered at 500Hz. Force curves were collected in dSPACE (dSPACE Inc., Wixom, MI) and Matlab (The MathWorks, Inc., Natick, MA) and analyzed later using Matlab.

Synthetic Procedures

General procedure for Luche dione reduction (used for compounds 1a-c and 2a):

Reduction of diones was adapted from a previous procedure.⁸ A solution of dione and cerium(III) chloride heptahydrate (2.0 equiv.) in anhydrous ethanol was cooled to 0°C in an ice-water bath with stirring for 30 min under N₂(g). Sodium borohydride (2.13 equiv.) was added in portions over 5 min. The reaction was stirred for 1 hr at 0°C, then carefully quenched with sat. NH₄Cl (aq.). The solution was brought to room temperature and extracted with ethyl acetate. The combined organic layers were washed with H₂O and brine, then dried over Na₂SO₄, filtered, and solvent was removed by rotary evaporation to give the crude diol. The diols were further purified via flash chromatography.

General procedure for esterification (used for compounds 1a-c and 2a):

Esterification of the diols was carried out using 4-pentenoiic anhydride in the presence of 4-dimethylaminopyridine in anhydrous THF. A solution of diol and 4-dimethylaminopyridine (1.8 equivalent) in anhydrous THF was sparged with N₂(g) for 30 min. while stirring. Anhydride (2.6 equiv.) was added dropwise via syringe and the reaction was stirred overnight. Excess anhydride was quenched with 1 mL MeOH. Purification by flash chromatography furnished the diesters.

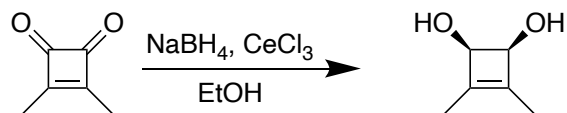
General procedure for Ring Closing Metathesis (RCM, used for all compounds):

Ring Closing Metathesis of CBE bis-alkenes was performed using Grubbs Catalyst 2nd generation in dilute (2 mM) dry DCM. A solution of Grubbs Catalyst 2nd generation (0.05 equiv.) in dry DCM was sparged with N₂(g) for 30 min. while stirring. To this solution was added dropwise a solution of the CBE bis-alkene in dry DCM. The reaction was stirred with continuous N₂(g) sparging and monitored by TLC until completion (2-4 hr). The reaction was opened to atmosphere and quenched with 2 mL of ethyl vinyl ether. DCM was removed *in vacuo* and the crude product was purified by flash chromatography.

General Procedure for Ring Opening Metathesis Polymerization (ROMP, used for all compounds):

CBE macrocycles were co-polymerized with freshly distilled 9-oxabicyclo[6.1.0]non-4-ene using Grubbs Catalyst 2nd Generation at a total monomer concentration of 1 M in dry DCM under N₂(g). A 2 mL crimp top vial was charged with the CBE macrocycle (0.25 equiv.) under N₂(g). Stock solutions of freshly distilled 9-oxabicyclo[6.1.0]non-4-ene and Grubbs Catalyst 2nd Generation in dry DCM were prepared and sparged with N₂(g) for 15 min. The epoxide solution (0.75 equiv.) was first added to the vial via air-tight syringe to dissolve the CBE macrocycle. Then, the Grubbs Catalyst solution (0.0005 equiv.) was added via air-tight syringe to initiate the polymerization. Typically, the polymerizations become very viscous after 10-15 min., causing the stir bar to stop spinning. When this

occurs, 0.1 mL of dry DCM is added via syringe and the reaction is stirred overnight. The polymerization was quenched with 20 drops of ethyl vinyl ether and then precipitated into methanol to give the crude polymer. Polymers were purified via two additional precipitation cycles and dried for one hour prior to use.

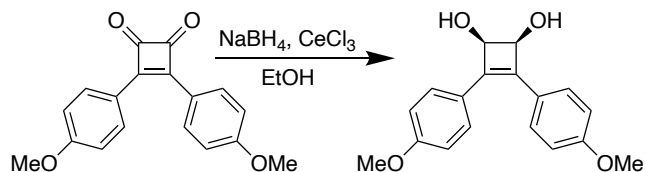


Synthesis of 2a-diol: The diketone was synthesized following a previous procedure.⁹ Reduction of the diketone (777 mg, 7.06 mmol, 1.0 equiv.) was performed with sodium borohydride (570 mg, 15.04 mmol, 2.13 equiv.) in the presence of cerium(III) chloride heptahydrate (5.26 g, 14.11 mmol, 2.0 equiv.) following the procedure described above to give **2a-diol** as pale yellow crystals (273 mg, 34%).

Physical State: pale-yellow crystals

¹H NMR (400 MHz, CDCl₃): δ 4.48 (s, 2H), 2.56 (b, 2H), 1.64 (s, 6H).

¹³C NMR (400 MHz, CDCl₃): δ 145.42, 73.06, 10.68.



HRMS-ESI (m/z): [M + H]⁺ calcd for C₆H₁₀O₂, 113.05971; found, 113.06006.

TLC: R_f = 0.21 (1:1 hexanes:EtOAc), visualized with KMnO₄ stain.

Synthesis of 1b-diol: The diketone was synthesized following a previous procedure.¹⁰ Reduction of the diketone (1.27 g, 4.3 mmol, 1.0 equiv.) was performed with sodium borohydride (170 mg, 4.6 mmol, 1.065 equiv.) in the presence of cerium(III) chloride heptahydrate (1.613 g, 4.3 mmol, 1.0 equiv.) following the procedure described above. Purification by flash chromatography (SiO₂, 4:1 hexanes:EtOAc) furnished **1b-diol** as a light yellow solid (80mg, 40%).

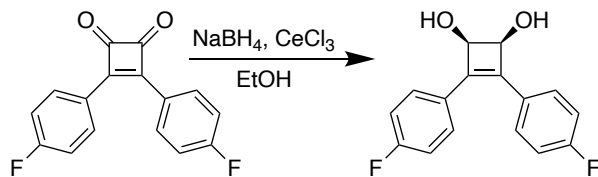
Physical State: light yellow solid

¹H NMR (400 MHz, CDCl₃): δ 7.55 (d, 4H), 6.83 (d, 4H), 4.90 (s, 2H), 3.80 (s, 6H), 3.70 (s, 2H).

¹³C NMR (101 MHz, CDCl₃): δ 159.72, 141.60, 128.64, 126.26, 113.97, 71.06, 55.35.

HRMS-ESI (m/z): [M + Na]⁺ calcd for C₁₈H₁₈O₄, 321.1097; found, 321.1099.

TLC: R_f = 0.16 (1:1 hexanes:EtOAc)

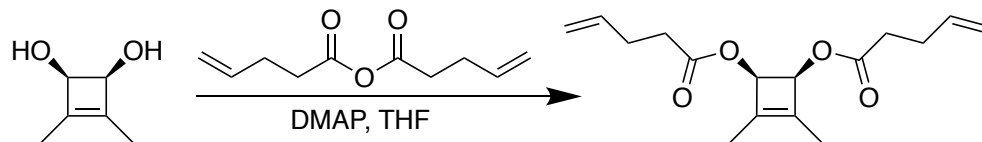


Synthesis of 1c-diol: The diketone was synthesized following a previous procedure.¹⁰ Reduction of the diketone (1.0 g, 3.70 mmol, 1.0 equiv.) was performed with sodium borohydride (298 mg, 7.88 mmol, 2.13 equiv.) in the presence of cerium(III) chloride heptahydrate (2.76 g, 7.40 mmol, 2.0 equiv.) following the procedure described above. Purification by flash chromatography (SiO₂, 4:1 hexanes:EtOAc) furnished **1c-diol** as a light yellow solid (152 mg, 15%).

Physical State: light yellow solid

¹H NMR (400 MHz, CDCl₃): δ 7.63 – 7.60 (m, 4H), 7.08 – 7.03 (m, 4H), 5.04 (s, 2H), 2.62 (s, 2H).

HRMS-ESI (m/z): [M - H]⁺ calcd for C₁₆H₁₂F₂O₂, 273.0722; found, 273.0762.



TLC: R_f = 0.27 (1:1 hexanes, EtOAc)

Synthesis of 2a-bisalkene: Esterification of **2a-diol** (269 mg, 2.36 mmol, 1 equivalent) was performed with 4-pentenoic anhydride (1.118 g, 6.14 mmol, 2.6 equivalent) following the procedure described above. Purification by flash chromatography (SiO₂, 9:1 hexanes:EtOAc) furnished **2a-bisalkene** as a colorless oil (400 mg, 61%).

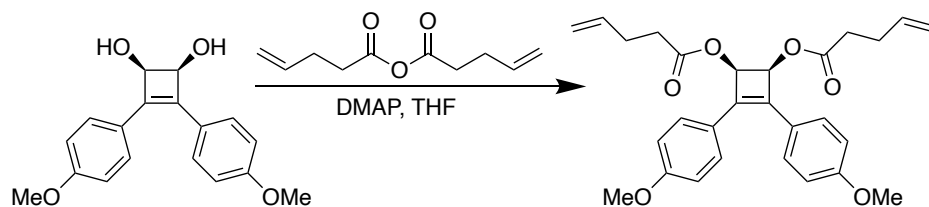
Physical State: colorless oil

¹H NMR (400 MHz, CDCl₃): δ 5.91 - 5.73 (m, 2H), 5.52 (s, 2H), 5.13 - 4.93 (m, 4H), 2.52 - 2.28 (m, 8H), 1.67 (s, 6H).

¹³C NMR (400 MHz, CDCl₃): δ 172.65, 143.36, 136.56, 115.51, 74.11, 33.46, 28.80, 11.29.

HRMS-ESI (m/z): [M + Na]⁺ calcd for C₁₆H₂₂O₄, 301.141; found, 301.1418.

TLC: $R_f = 0.24$ (9:1 hexanes:EtOAc), visualized with KMnO_4 stain.

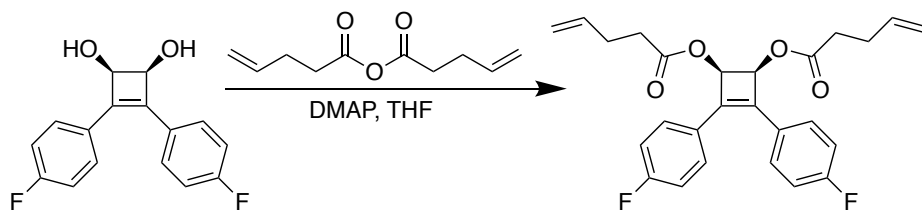


Synthesis of 1b-bisalkene: Esterification of **1b-diol** (100 mg, 0.33 mmol, 1 equivalent) was performed with 4-pentenoic anhydride (156 mg, 0.86 mmol, 2.6 equivalent) following the procedure described above. Purification by flash chromatography (SiO_2 , 4:1 hexanes:EtOAc) furnished **6c** as a colorless oil (138mg, 90%).

Physical State: colorless oil

^1H NMR (400 MHz, CDCl_3): δ 7.52 (d, 4H), 6.87 (d, 4H), 6.15 (s, 2H), 5.88 - 5.76 (m, 2H), 5.09 - 4.97 (m, 4H), 3.82 (s, 6H), 2.51 - 2.35 (m, 8H).

^{13}C NMR (101 MHz, CDCl_3): δ 172.72, 160.19, 139.00, 136.57, 136.38, 128.74, 125.03,



115.79, 115.70, 114.05, 71.71, 55.36, 33.64, 33.37, 28.87, 28.57.

HRMS-ESI (m/z): $[\text{M} + \text{Na}]^+$ calcd for $\text{C}_{28}\text{H}_{30}\text{O}_6$, 485.1935; found, 485.1926.

TLC: $R_f = 0.54$ (1:1 hexanes:EtOAc)

Synthesis of 1c-bisalkene: Esterification of **1c-diol** (98 mg, 0.36 mmol, 1 equivalent) was performed with 4-pentenoic anhydride (169 mg, 0.93 mmol, 2.6 equivalent) following the procedure described above. Purification by flash chromatography (SiO_2 , 4:1 hexanes:EtOAc) furnished **1c-bisalkene** as a colorless oil (114mg, 73%).

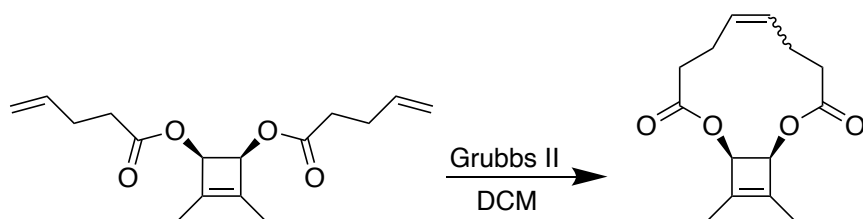
Physical State: colorless oil

^1H NMR (400 MHz, CDCl_3): δ 7.59 - 7.45 (m, 4H), 7.03 (t, $J = 8.7$ Hz, 4H), 6.15 (s, 2H), 5.90 - 5.69 (m, 2H), 5.14 - 4.84 (m, 4H), 2.57 - 2.26 (m, 8H).

¹³C NMR (101 MHz, CDCl₃): δ 172.42, 164.30, 161.81, 140.67, 140.07, 136.33, 129.21, 129.13, 128.06, 128.03, 115.94, 115.72, 115.69, 71.48, 33.45, 28.71.

HRMS-ESI (m/z): [M + Na]⁺ calcd for C₂₆H₂₄F₂O₄, 461.1535; found, 461.1584.

TLC: R_f = 0.72 (1:1 hexanes:EtOAc)



Synthesis of 2a-macrocyclic: RCM of **2a-bisalkene** was performed following the procedure described above. A solution of Grubbs catalyst 2nd generation (61 mg, 0.072 mmol, 0.05 equivalent) in dichloromethane (710 mL) was sparged with N₂(g) for 30 minutes while stirring. To this solution was added dropwise a solution of **2a-bisalkene** (400 mg, 1.44 mmol, 1 equivalent) in dichloromethane (10 mL). Purification by flash chromatography (SiO₂, 9:1 hexanes:EtOAc) furnished compound **2a-macrocyclic** as a white solid (327 mg, 90%).

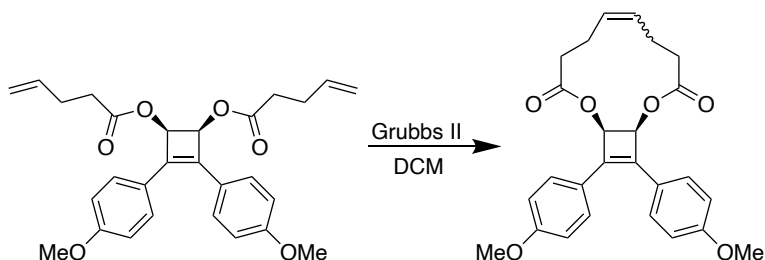
Physical State: white solid

¹H NMR (500 MHz, CDCl₃): δ 5.64 - 5.43 (m, 3H), 5.39 - 5.27 (m, 1H), 2.77 - 2.07 (m, 8H), 1.63 (s, 6H).

¹³C NMR (400 MHz, CDCl₃): δ 172.62, 172.11, 143.01, 142.81, 130.13, 129.18, 74.08, 73.84, 35.09, 34.81, 27.22, 23.50, 11.22, 11.13.

HRMS-ESI (m/z): [M + H]⁺ calcd for C₁₄H₁₈O₄, 251.1278; found, 251.1281.

TLC: R_f = 0.48 (1:1 hexanes:EtOAc), visualized with KMnO₄ stain.



Synthesis of 1b-macrocycle: RCM of **1c-bisalkene** (138 mg, 0.3 mmol, 1 equivalent) was performed with Grubbs catalyst 2nd generation (13 mg, 0.015 mmol, 0.05 equivalent) following the procedure described above. Purification by flash chromatography (SiO₂, 4:1 hexanes:EtOAc) furnished **1c-macrocycle** as a white solid (89mg, 69%).

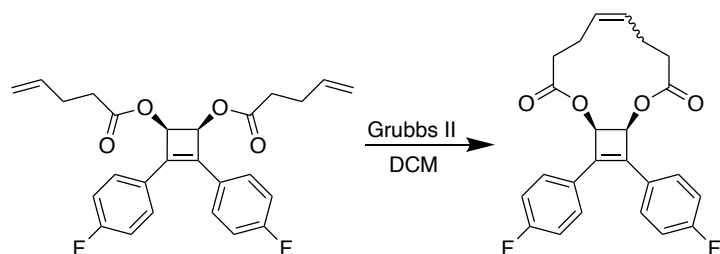
Physical State: white solid

¹H NMR (400 MHz, CDCl₃): δ 7.52 - 7.48 (m, 4H), 6.89 - 6.85 (m, 4H), 6.23 - 6.21 (m, 2H), 5.59 - 5.40 (m, 2H), 3.82 (s, 6H), 2.84 - 2.10 (m, 8H).

¹³C NMR (101 MHz, CDCl₃): δ 172.69, 172.01, 160.16, 138.97, 138.78, 130.29, 129.23, 128.61, 128.60, 125.12, 114.09, 114.07, 71.61, 71.34, 55.37, 55.36, 35.51, 34.99, 27.11, 23.63.

HRMS-ESI (m/z): [M + H]⁺ calcd for C₂₆H₂₆O₆, 435.1802; found, 435.18027

TLC: R_f = 0.52 (1:1 hexanes:EtOAc)



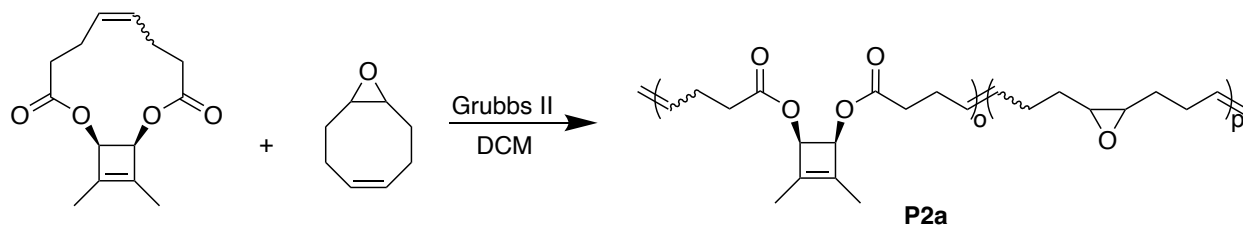
Synthesis of 1c-macrocycle: RCM of **1c-bisalkene** (119 mg, 0.27 mmol, 1 equivalent) was performed with Grubbs catalyst 2nd generation (11.5 mg, 0.014 mmol, 0.05 equivalent) following the procedure described above. Purification by flash chromatography (SiO₂, 4:1 hexanes:EtOAc) furnished **1c-macrocycle** as a white solid (106mg, 95%).

¹H NMR (400 MHz, CDCl₃): δ 7.53 - 7.39 (m, 4H), 7.04 - 6.88 (m, 4H), 6.23 - 6.09 (m, 2H), 5.58 - 5.46 (m, 1H), 5.40 - 5.27 (m, 1H), 2.80 - 1.99 (m, 8H).

¹³C NMR (101 MHz, CDCl₃): δ 172.33, 171.67, 164.20, 161.71, 139.98, 139.80, 130.17, 129.10, 129.06, 129.02, 128.98, 128.20, 128.17, 71.41, 71.13, 35.25, 34.77, 26.99, 23.47.

HRMS-ESI (m/z): [M + H]⁺ calcd for C₂₄H₂₀F₂O₄, 411.1402; found, 411.14021.

TLC: R_f = 0.64 (1:1 hexanes:EtOAc)

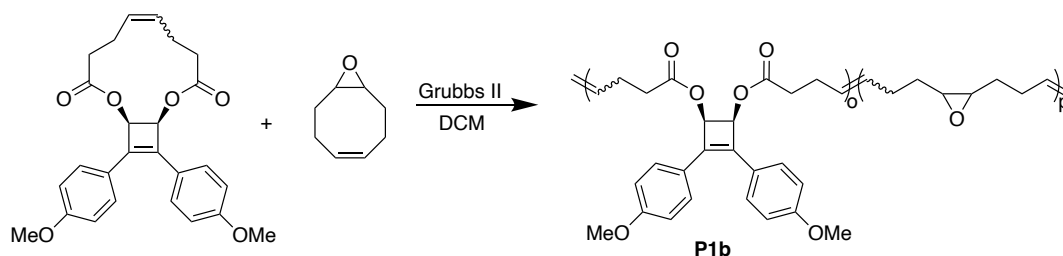


Synthesis of P2a: Cyclobutene **2a-macrocycle** was co-polymerized with freshly distilled 9-oxabicyclo[6.1.0]non-4-ene using Grubbs Catalyst 2nd Generation according to the above procedure. For SMFS experiments, the polymer was further purified via one additional reverse precipitation from DCM according to literature precedent.

Physical State: white, gummy polymer

¹H NMR (400 MHz, CDCl₃): δ 5.59 - 5.34 (m, 5.6H), 2.92 (s, 2H), 2.47 - 2.05 (m, 12.12H), 1.75 - 1.45 (m, 12.26H).

Polymer	χ_{CBE}	$\chi_{\text{epoxy COD}}$	M_n (kDa)	M_w (kDa)	\bar{D}
P2a-1 ⁴⁰⁷⁹	0.20	0.80	89	109	1.2
P2a-2 ^{4068,son}	0.34	0.66	82	142	1.7



Synthesis of P1b: Cyclobutene **1b-macrocycle** was co-polymerized with 9-oxabicyclo[6.1.0]non-4-ene following the ROMP polymerization procedure described above.

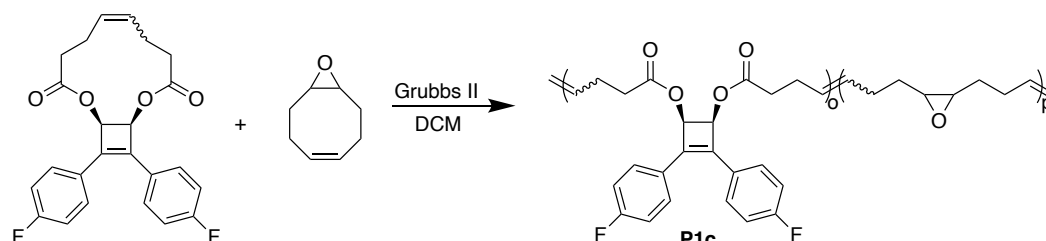
Physical State: white, gummy polymer

¹H NMR (400 MHz, CDCl₃): δ 7.52 (d, J = 8.1 Hz, 4H), 6.87 (d, J = 8.2 Hz, 4H), 6.13 (s, 2H), 5.57 - 5.35 (m, 11H), 3.82 (s, 6H), 2.92 (s, 7H), 2.48 - 2.01 (m, 44H), 1.62 - 1.50 (m, 28H).

^{13}C NMR (101 MHz, CDCl_3): δ 172.49, 129.93, 129.38, 128.83, 128.61, 113.95, 74.56, 56.68, 55.27, 29.56, 27.81.

dn/dc (THF): 0.1033

	χ_{CBE}	$\chi_{\text{epoxy COD}}$	M_n (kDa)	M_w (kDa)	PDI
P1b-1	0.160	0.840	83.0	127	1.5



Synthesis of P1c: Cyclobutene **1c-macrocycle** was co-polymerized with 9-oxabicyclo[6.1.0]non-4-ene following the ROMP polymerization procedure described above.

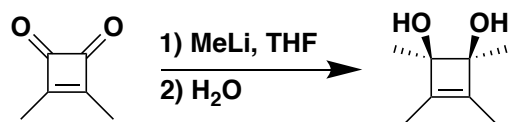
Physical State: white, gummy polymer

^1H NMR (400 MHz, CDCl_3): δ 7.60 - 7.46 (m, 2H), 7.11 - 6.97 (m, 2H), 6.13 (s, 1H), 5.62 - 5.33 (m, 5H), 2.91 (s, 2H), 2.57 - 1.99 (m, 19H), 1.70 - 1.43 (m, 9H).

^{13}C NMR (101 MHz, CDCl_3): δ 172.78, 129.92, 129.38, 129.19, 129.10, 128.67, 115.94, 115.73, 71.43, 56.67, 29.55, 27.79.

dn/dc (THF): 0.1304

P1c	χ_{CBE}	$\chi_{\text{epoxy COD}}$	M_n (kDa)	M_w (kDa)	PDI
P1c-1	0.180	0.820	35.1	59.1	1.7
P1c-2	0.160	0.840	75.5	126	1.7



Synthesis of 2b-diol: Synthesis of **2b-diol** was adapted from prior literature.¹¹ Diketone (660 mg, 6 mmol, 1 eq.) was dissolved in 20 mL of anhydrous THF and cooled to -78 °C while sparging with N_2 (g). MeLi (1.6M in Et_2O , 11.3 mL, 18 mmol, 3 eq.) was

then added dropwise. After reacting at $-78\text{ }^{\circ}\text{C}$ for one hour, 10 mL of water was added dropwise. After 10 minutes, the reaction mixture was allowed to warm to room temperature and was subsequently extracted with ethyl acetate (20 mL x 3). The combined organic layers were washed with H_2O (20 mL x 1) and brine (20 mL x 1) and subsequently dried over Na_2SO_4 . Purification by flash chromatography (SiO_2 , 1:1 hexanes:EtOAc) furnished compound **2b-diol** as a white solid (290 mg, 34%).

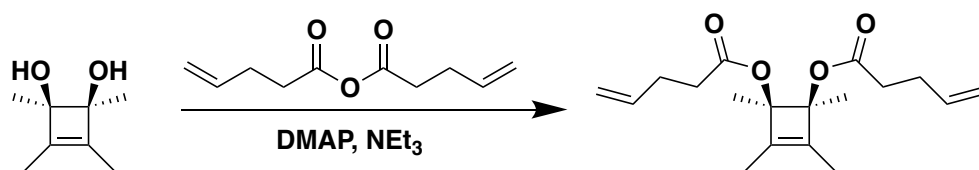
Physical State: white solid

^1H NMR (500 MHz, CDCl_3): δ 2.36 (b, 2H), 1.56 (s, 6H), 1.27 (s, 6H).

^{13}C NMR (500 MHz, CDCl_3): δ 144.27, 79.94, 18.54, 7.60.

HRMS-ESI (m/z): $[\text{M} + \text{Na}]^+$ calcd for $\text{C}_8\text{H}_{14}\text{O}_2$, 165.0886; found, 165.0884.

TLC: $R_f = 0.3$ (1:1 hexanes:EtOAc), visualized with KMnO_4 stain.



Synthesis of 2b-bisalkene: Synthesis of **2b-bisalkene** was adapted from prior literature.¹² To a 20 mL scintillation vial containing diol **2** (270 mg, 1.9 mmol, 1 eq.), 4-dimethylaminopyridine (418 mg, 3.4 mmol, 1.8 eq.), and triethylamine (0.95 mL, 6.8 mmol, 3.6 eq.) was added 4-pentenoic anhydride (0.87 mL, 4.7 mmol, 2.5 eq.). The solution was stirred at room temperature under an atmosphere of $\text{N}_2(\text{g})$ for 16 hours. MeOH (3 mL) was added to quench the reaction and the solution was diluted with 20 mL of ethyl acetate. The solution was washed with 1M aqueous HCl (5 mL), saturated aqueous NaHCO_3 (5 mL), water (5 mL) and brine (5 mL). After drying over Na_2SO_4 , purification by flash chromatography (SiO_2 , 4:1 hexanes:EtOAc) furnished compound **2b-bisalkene** as a colorless oil (330 mg, 57%).

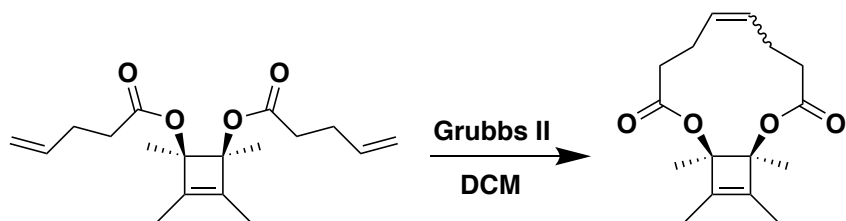
Physical State: colorless oil

^1H NMR (500 MHz, CDCl_3): δ 5.88 – 5.76 (m, 2H), 5.09 – 4.94 (m, 4H), 2.37 – 2.32 (m, 8H), 1.66 (s, 6H), 1.55 (s, 6H).

^{13}C NMR (500 MHz, CDCl_3): δ 172.04, 144.43, 136.82, 115.34, 86.68, 34.12, 28.90, 16.80, 9.74.

HRMS-ESI (m/z): $[\text{M} + \text{H}]^+$ calcd for $\text{C}_{18}\text{H}_{26}\text{O}_4$, 307.1904; found $[\text{M} + \text{Na}]^+$, 329.1730.

TLC: $R_f = 0.67$ (1:1 hexanes:EtOAc), visualized with KMnO_4 stain.



Synthesis of 2b-macrocycle: Cyclization of **2b-bialkene** (318 mg, 1 mmol, 1 equivalent) was performed with Grubbs catalyst 2nd generation (44 mg, 0.05 mmol, 0.05 equivalent) following the procedure described above. Purification by flash chromatography (SiO₂, 4:1 hexanes:EtOAc) furnished **2b-macrocycle** as an off-white solid (220 mg, 79%). Recrystallization in hexane yielded white crystals (147 mg, 53%).

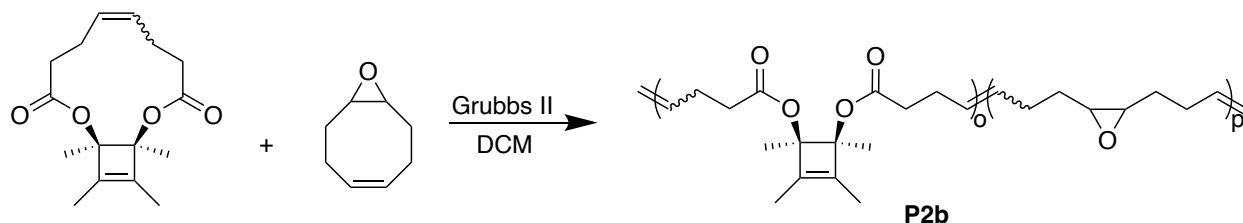
Physical State: white crystals

¹H NMR (500 MHz, CDCl₃), mixture of isomers: δ 5.57 – 5.28 (m, 2H), 2.63 – 2.10 (m, 8H), 1.66 (m, 6H), 1.53 – 1.51 (m, 6H).

¹³C NMR (500 MHz, CDCl₃), mixture of isomers: δ 172.00, 171.90, 144.13, 143.71, 129.70, 129.19, 86.91, 86.63, 36.10, 35.04, 27.36, 22.92, 17.19, 16.79, 9.70, 9.45.

HRMS-ESI (m/z): [M + H]⁺ calcd for C₁₆H₂₂O₄, 279.1591; found, 279.1598.

TLC: R_f = 0.4 (4:1 hexanes:EtOAc), visualized with KMnO₄ stain.

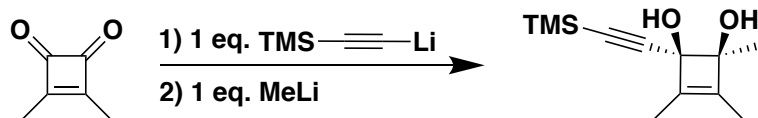


Synthesis of polymer P2b: Polymer **P2-b** was synthesized in the same manner as polymer **P2-a**.

Physical State: white, gummy polymer

¹H NMR (500 MHz, CDCl₃): δ 5.56 – 5.34 (m, 2H), 2.94 – 2.90 (m, 1.71H), 2.38 – 2.08 (m, 4.52H), 1.66 (s, 0.75H), 1.61 – 1.52 (m, 4.42H).

Polymer	χ_{CBE}	$\chi_{\text{epoxy COD}}$	M_n (kDa)	M_w (kDa)	\bar{D}
P2b	0.13	0.87	241	298	1.2



Synthesis of 2c-diol: Synthesis of **2c-diol** was prepared in a similar manner to **2b-diol**. Diketone (1.2 g, 10.9 mmol, 1 eq.) was dissolved in 20 mL of anhydrous THF and cooled to $-78\text{ }^{\circ}\text{C}$ while sparging with N_2 (g). Lithium (trimethylsilyl)acetylide solution (0.5M in THF, 22 mL, 10.9 mmol, 1 eq.) was then added dropwise. After reacting at $-78\text{ }^{\circ}\text{C}$ for 2 hours, MeLi (1.6M in Et_2O , 7.5 mL, 12 mmol, 1.1 eq.) was then added dropwise. After reacting at $-78\text{ }^{\circ}\text{C}$ for one hour, 10 mL of water was added dropwise. After 10 minutes, the reaction mixture was allowed to warm to room temperature and was subsequently extracted with ethyl acetate (20 mL x 3). The combined organic layers were washed with H_2O (20 mL x 1) and brine (20 mL x 1) and subsequently dried over Na_2SO_4 . Purification by flash chromatography (SiO_2 , 1:1 hexanes:EtOAc) furnished compound **2c-diol** as a white solid (50 mg, 2%).

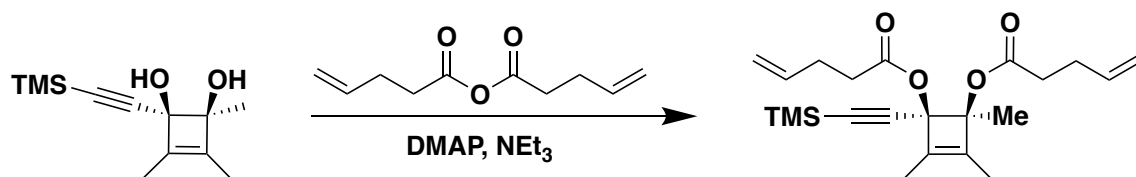
Physical State: white solid

^1H NMR (500 MHz, CDCl_3): δ 2.81 (b, 1H), 2.57 (b, 1H), 1.64 (s, 3H), 1.60 (s, 3H), 1.40 (s, 3H), 0.16 (s, 9H).

^{13}C NMR (500 MHz, CDCl_3): δ 148.17, 141.73, 140.48, 136.89, 92.65, 79.70, 19.58, 8.21, 8.16, 0.75.

HRMS-ESI (m/z): $[\text{M} + \text{Na}]^+$ calcd for $\text{C}_{12}\text{H}_{20}\text{O}_2\text{Si}$, 247.1125; found, 247.1127.

TLC: $R_f = 0.6$ (1:1 hexanes:EtOAc), visualized with KMnO_4 stain.



Synthesis of 2c-bisalkene: Synthesis of **2c-bisalkene** was performed in the same manner as **2b-bisalkene**. Purification by flash chromatography (SiO_2 , 4:1 hexanes:EtOAc) furnished compound **2c-bisalkene** as a colorless oil (43%).

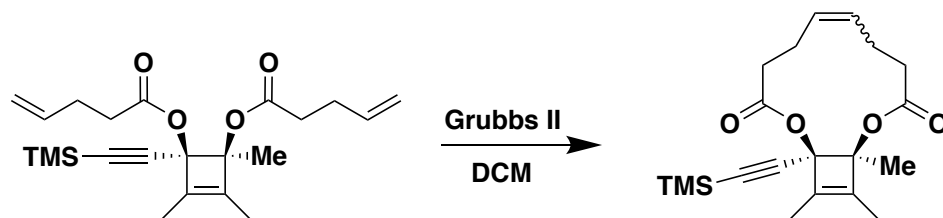
Physical State: colorless oil

^1H NMR (500 MHz, CDCl_3): δ 5.88 – 5.75 (m, 2H), 5.09 – 4.97 (m, 4H), 2.45 – 2.29 (m, 8H), 1.73 – 1.70 (m, 9H), 0.16 (s, 9H).

^{13}C NMR (500 MHz, CDCl_3): δ 171.86, 170.69, 147.40, 141.85, 136.69, 136.60, 115.47, 115.45, 99.30, 94.13, 86.36, 80.07, 34.14, 33.55, 28.85, 28.72, 18.12, 11.20, 9.25, -0.18.

HRMS-ESI (m/z): $[M + Na]^+$ calcd for $C_{22}H_{32}O_4Si$, 411.1962; found $[M + Na]^+$, 411.1969.

TLC: $R_f = 0.45$ (4:1 hexanes:EtOAc), visualized with $KMnO_4$ stain.



Synthesis of 2c-macrocycle: Synthesis of **2c-macrocycle** was performed in the same manner as **2a-** and **2b-macrocycles**. Purification by flash chromatography (SiO_2 , 4:1 hexanes:EtOAc) furnished compound **2c-macrocycle** as a colorless oil (60%).

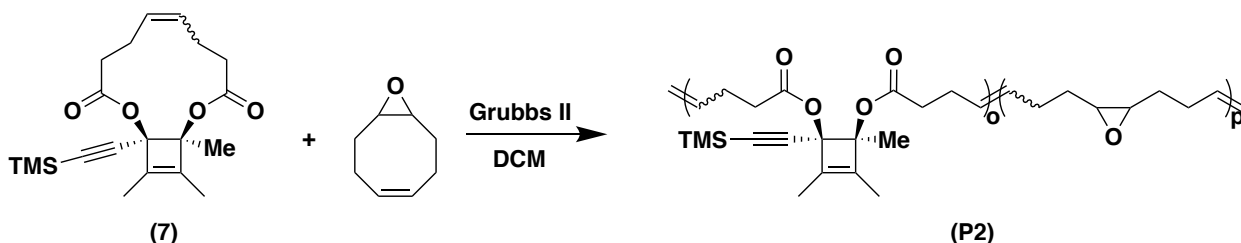
Physical State: white crystals

1H NMR (500 MHz, $CDCl_3$), mixture of isomers: δ 5.62 – 5.27 (m, 2H), 2.68 – 2.09 (m, 8H), 1.74 – 1.64 (m, 9H), 0.15 (s, 9H).

^{13}C NMR (500 MHz, $CDCl_3$), mixture of isomers: δ 172.24, 171.83, 171.25, 170.71, 147.46, 141.65, 140.57, 130.79, 130.27, 129.13, 128.54, 99.56, 99.52, 94.04, 93.89, 86.93, 86.69, 80.66, 36.72, 35.17, 35.12, 34.88, 27.70, 27.60, 23.91, 22.41, 19.21, 18.46, 11.49, 11.23, 9.33, 9.06.

HRMS-ESI (m/z): $[M + H]^+$ calcd for $C_{20}H_{28}O_4Si$, 361.1830; found $[M + H]^+$, 361.1835.

TLC: $R_f = 0.4$ (4:1 hexanes:EtOAc), visualized with $KMnO_4$ stain.



Synthesis of polymer P2c: Polymer **P2c** was synthesized in the same manner as polymers **P2a** and **P2b**.

Physical State: white, gummy polymer

1H NMR (500 MHz, $CDCl_3$): δ 5.54 – 5.33 (m, 2H), 2.93 – 2.91 (m, 1.68H), 2.39 – 2.09 (m, 4.62H), 1.76 – 1.68 (m, 1.4H), 1.62 – 1.48 (m, 5.1H), 0.16 (s, 1.32H).

Polymer	χ_{CBE}	$\chi_{epoxy\ COD}$	M_n (kDa)	M_w (kDa)	\bar{D}
P2c	0.17	0.83	56	84	1.5

Summary of Polymer Characterization Data

Table S1. Summary of polymer compositions provided in individual synthetic experimentals, above.

Polymer	χ_{CBE}	$\chi_{\text{epoxy COD}}$	M_n (kDa)	M_w (kDa)	\bar{D}
P1b-1	0.16	0.84	83.0	127	1.5
P1c-1	0.18	0.82	35.1	59.1	1.7
P1c-2	0.16	0.84	75.5	126	1.7
P2a-1 ⁴⁰⁷⁹	0.20	0.80	89	109	1.2
P2a-2 ^{4068,son}	0.34	0.66	82	142	1.7
P2b	0.13	0.87	241	298	1.2
P2c	0.17	0.83	56	84	1.5

Modeling of Mechanophore-Embedded Polymer Extension

Modeling of Monomer Contour Lengths

The detailed procedure of modeling of the contour lengths of the repeating units has been described previously.² The modeling was performed using Spartan® software. The equilibrium conformers of the molecules were minimized at the molecular mechanics level of theory. The end-to-end distance of the molecule was constrained until the bonding geometries were noticeably distorted. CoGEF (constrained geometry simulates external force)¹³ plots of energy as a function of displacement (blue-dot to blue-dot, below) was then obtained by shortening the constraint in 0.1 Å increments. The incremental change in energy ($E_n - E_{n-1}$) vs. change in distance ($d_n - d_{n-1}$) was taken as the force at the midpoint of the increment, and the resulting force vs. displacement curve was extrapolated to zero force to give a force-free contour length, (l_1) or (l_2).

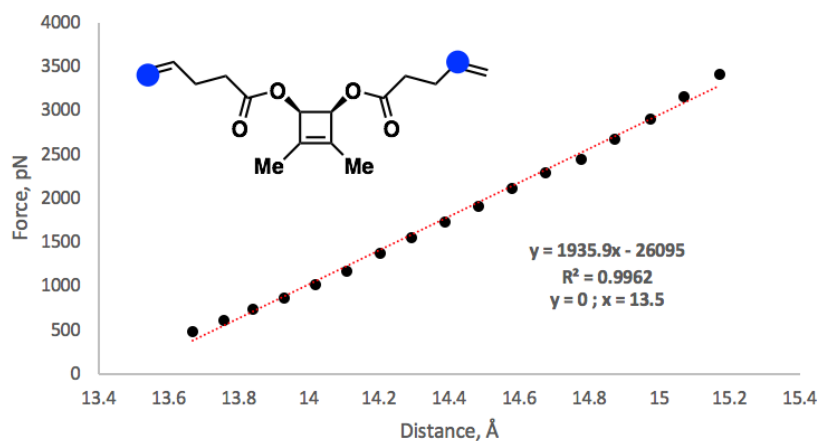


Figure S1. Monomer CBE-2a in its unreacted form and the corresponding force vs. displacement curve obtained by CoGEF. Fitting the curve (red line) provides l_1 as the x-intercept: $l_1 = 13.5$ Å.

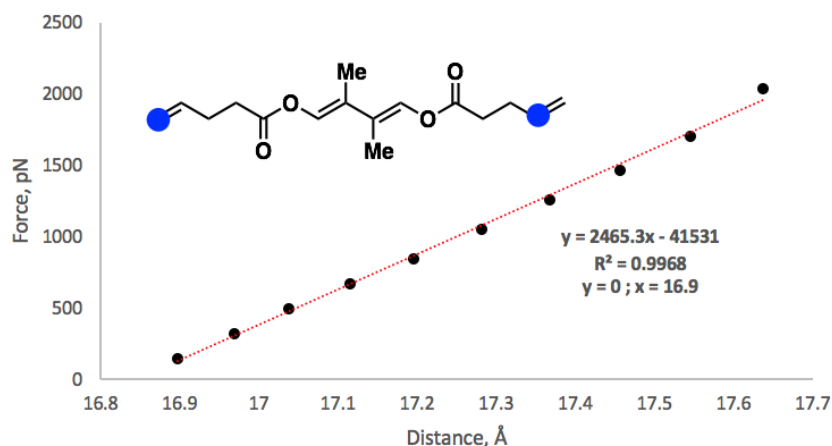


Figure S2. Monomer CBE-2a in its *E,E*-butadiene form and the corresponding force vs. displacement curve obtained by CoGEF. Fitting the curve (red line) provides l_2 as the x-intercept: $l_2 = 16.9 \text{ \AA}$.

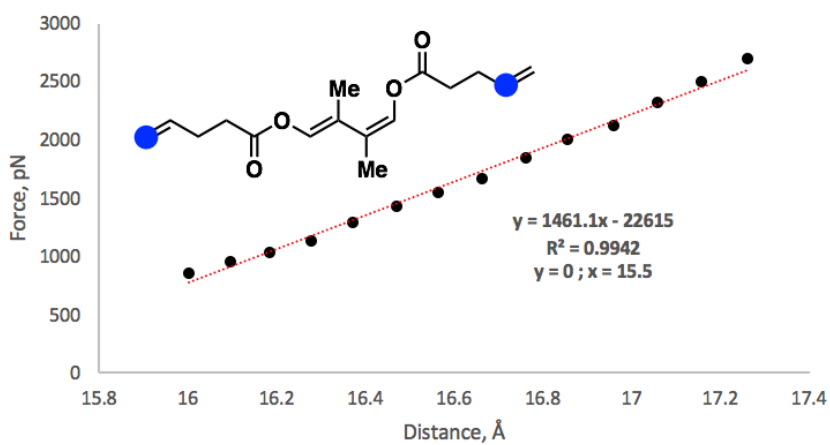


Figure S3. Monomer CBE-2a in its *E,Z*-butadiene form and the corresponding force vs. displacement curve obtained by CoGEF. Fitting the curve (red line) provides l_2 as the x-intercept: $l_2 = 15.5 \text{ \AA}$.

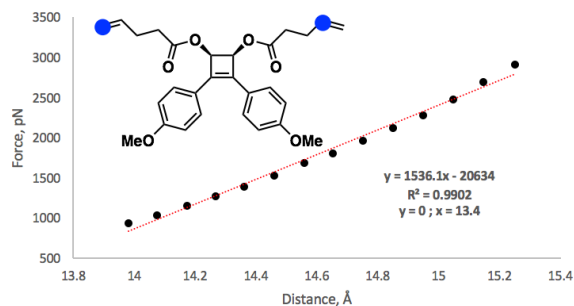


Figure S4: Monomer CBE-1b in its unreacted form and the corresponding force vs. displacement curve obtained by CoGEF. Fitting the curve (red line) provides l_1 as the x-intercept: $l_1 = 13.4 \text{ \AA}$.

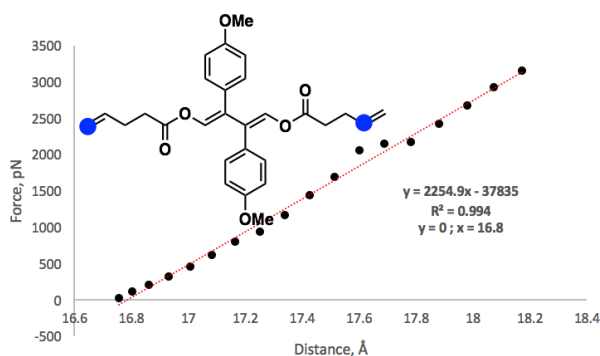


Figure S5: Monomer CBE-1b in its *E,E*-butadiene form and the corresponding force vs. displacement curve obtained by CoGEF. Fitting the curve (red line) provides l_2 as the x-intercept: $l_2 = 16.8 \text{ \AA}$.

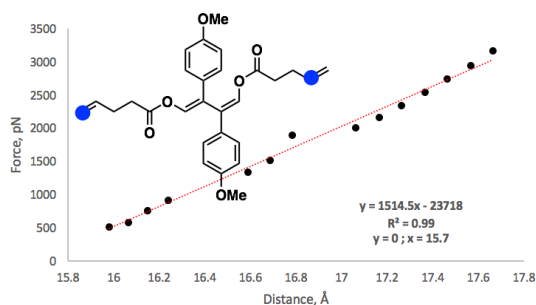


Figure S6: Monomer CBE-1b in its *E,Z*-butadiene form and the corresponding force vs. displacement curve obtained by CoGEF. Fitting the curve (red line) provides l_2 as the x-intercept: $l_2 = 15.7 \text{ \AA}$.

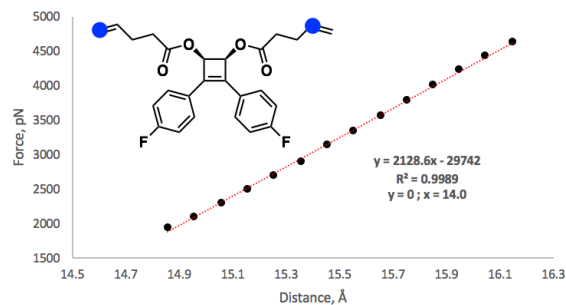


Figure S7: Monomer CBE-1c in its unreacted form and the corresponding force vs. displacement curve obtained by CoGEF. Fitting the curve (red line) provides l_1 as the x-intercept: $l_1 = 14.0 \text{ \AA}$.

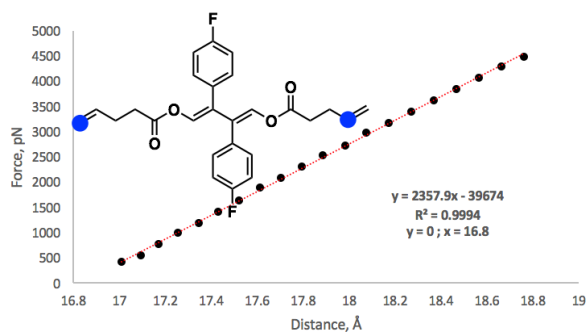


Figure S8: Monomer CBE-1c in its *E,E*-butadiene form and the corresponding force vs. displacement curve obtained by CoGEF. Fitting the curve (red line) provides l_2 as the x-intercept: $l_2 = 16.8 \text{ \AA}$.

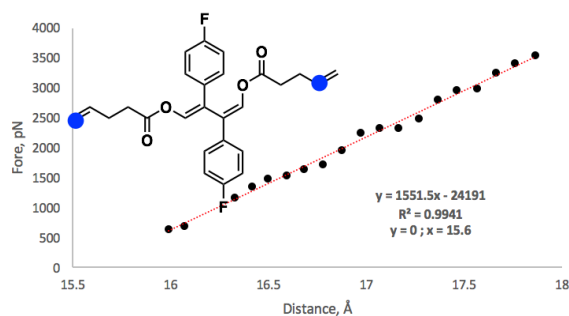


Figure S9: Monomer CBE-1c in its *E,Z*-butadiene form and the corresponding force vs. displacement curve obtained by CoGEF. Fitting the curve (red line) provides l_2 as the x-intercept: $l_2 = 15.6 \text{ \AA}$.

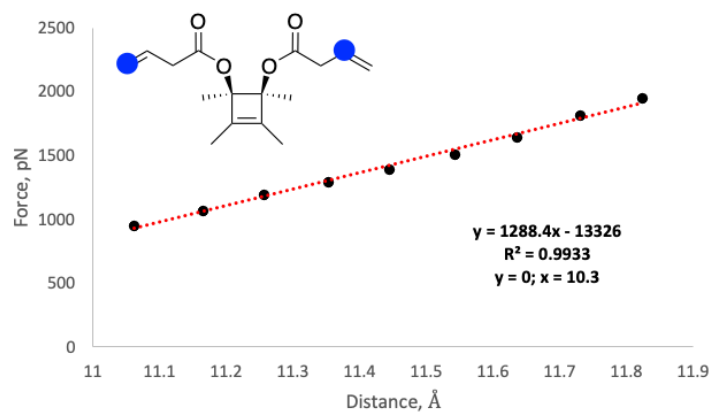


Figure S10. Monomer CBE-2b in its unreacted form and the corresponding force vs. displacement curve obtained by CoGEF. Fitting the curve (red line) provides l_1 as the x-intercept: $l_1 = 10.3 \text{ \AA}$.

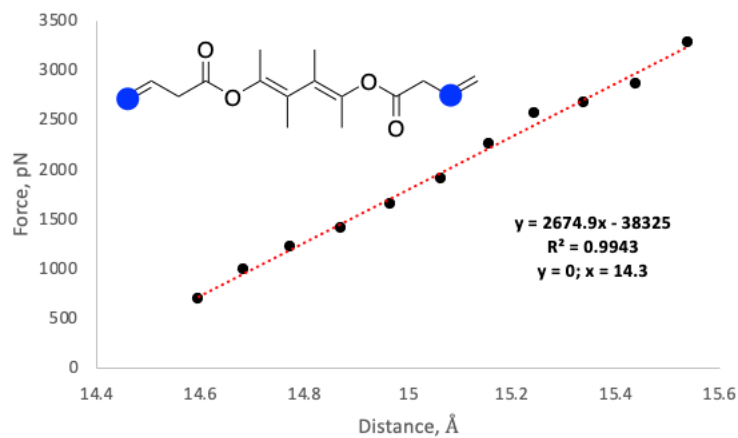


Figure S11. Monomer CBE-2b in its *E,E*-butadiene form and the corresponding force vs. displacement curve obtained by CoGEF. Fitting the curve (red line) provides l_2 as the x-intercept: $l_2 = 14.3 \text{ \AA}$.

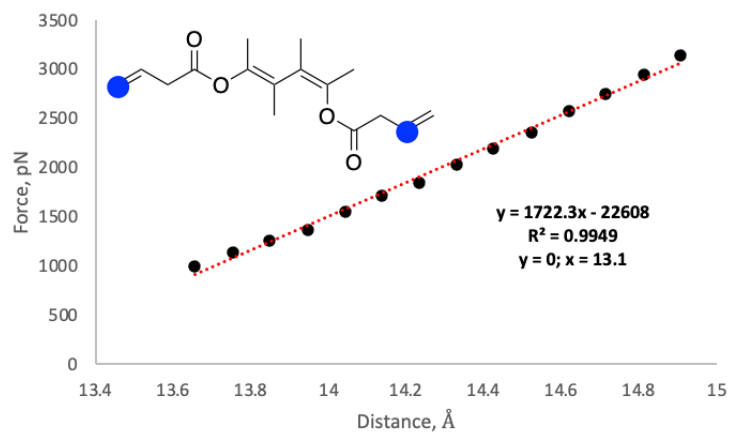


Figure S12. Monomer CBE-2b in its *E,Z*-butadiene form and the corresponding force vs. displacement curve obtained by CoGEF. Fitting the curve (red line) provides l_2 as the x-intercept: $l_2 = 13.1 \text{ \AA}$.

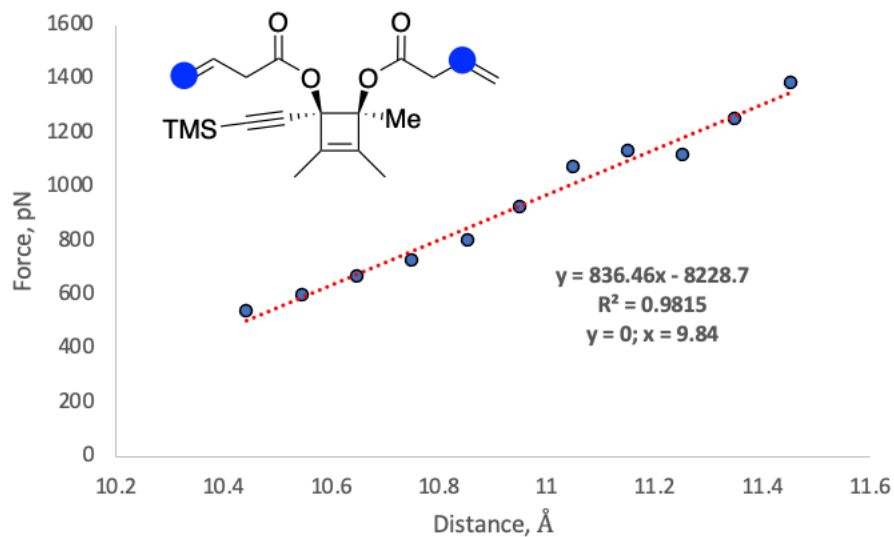


Figure S13. Monomer CBE-2c in its unreacted form and the corresponding force vs. displacement curve obtained by CoGEF. Fitting the curve (red line) provides l_1 as the x-intercept: $l_1 = 9.84 \text{ \AA}$.

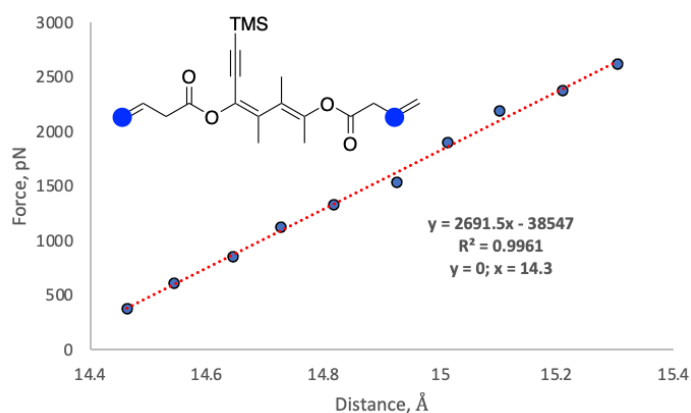


Figure S14. Monomer CBE-2c in its *E,E*-butadiene form and the corresponding force vs. displacement curve obtained by CoGEF. Fitting the curve (red line) provides l_2 as the x-intercept: $l_2 = 14.3$ Å.

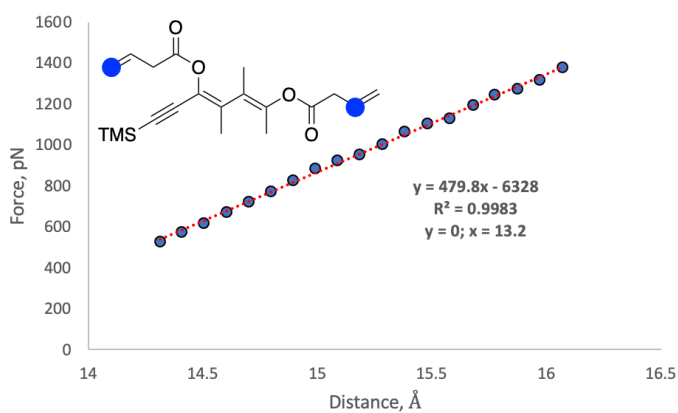


Figure S15. Monomer CBE-2c in its *E,Z*-butadiene form and the corresponding force vs. displacement curve obtained by CoGEF. Fitting the curve (red line) provides l_2 as the x-intercept: $l_2 = 13.2$ Å.

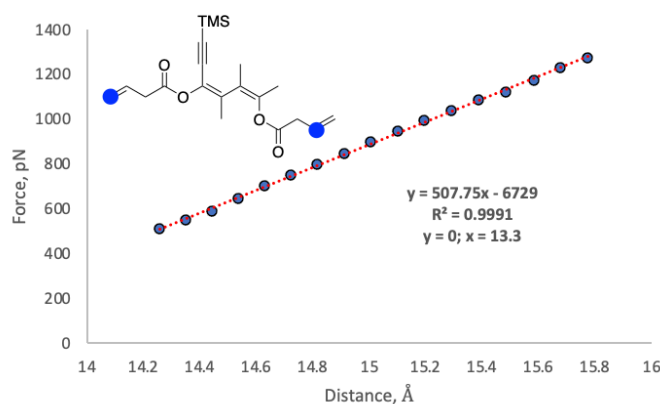


Figure S16. Monomer CBE-2c in its *Z,E*-butadiene form and the corresponding force vs. displacement curve obtained by CoGEF. Fitting the curve (red line) provides l_2 as the x-intercept: $l_2 = 13.3 \text{ \AA}$.

Summary of Monomer Extension Data.

Mechanophore	CBE Reactant (Å)	EE Ring-Opened Product (Å)	EZ Ring-Opened Product (Å)	ZE Ring-Opened Product (Å)
CBE-1b	13.4	16.8	15.7	-
CBE-1c	14.0	16.8	15.6	-
CBE-2a	13.5	16.9	15.5	-
CBE-2b	10.3	14.3	13.1	-
CBE-2c	0.98	14.3	13.2	13.3

The ratio of polymer contour lengths, L_2/L_1 , are obtained from the following equation,

$$\frac{L_2}{L_1} = \frac{(l_{butadiene} \times \chi_{butadiene}) + (l_{epoxy\ COD} \times \chi_{epoxy\ COD})}{(l_{CBE} \times \chi_{CBE}) + (l_{epoxy\ COD} \times \chi_{epoxy\ COD})}$$

where χ denotes the mole fraction of CBE or epoxy-COD within the polymer as determined by $^1\text{H-NMR}$ spectroscopy, and l refers to the end-to-end distance obtained from CoGEF calculations for the various monomers.

Polymer	%CBE	<i>L2/L1</i> (Modelin g-EE)	<i>L2/L1</i> (Modelin g-EZ)	<i>L2/L1</i> (Modelin g-ZE)
P2a	0.17	1.06	1.04	-
P2b	0.13	1.05	1.04	-
P2c	0.17	1.08	1.06	1.06

Details of Constant-Velocity SMFS Analysis

Determination of Polymer Extension by Fitting to a FJC Model

The contour lengths of the polymers before and after transition were determined by fitting the pre- and post- transition force curves to an extended freely jointed chain (FJC) model as described previously.¹⁻² Such a fit allows the determination of polymer chain lengths corresponding to the initial state, when active mechanophores are intact ($L1$), and the final state, when all mechanophores have undergone an irreversible ring-opening reaction ($L2$).

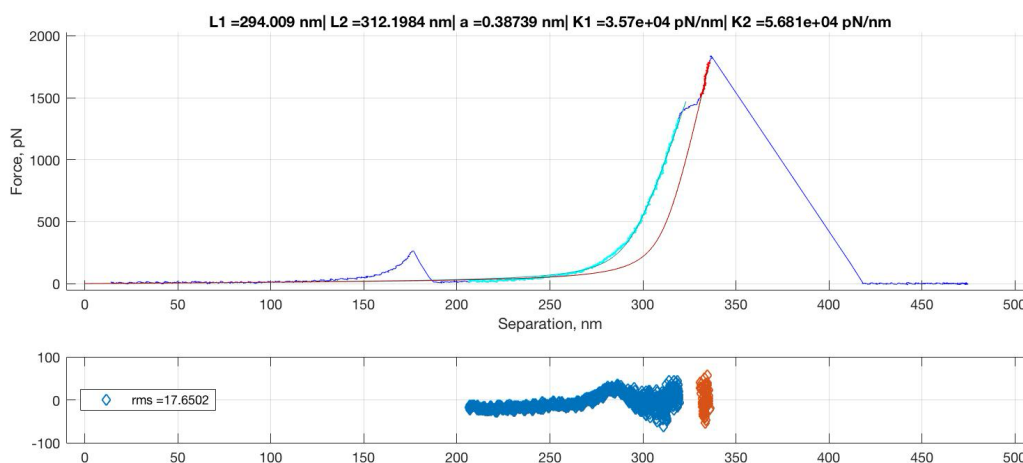


Figure S17: Representative FJC fitting of polymer P2a.

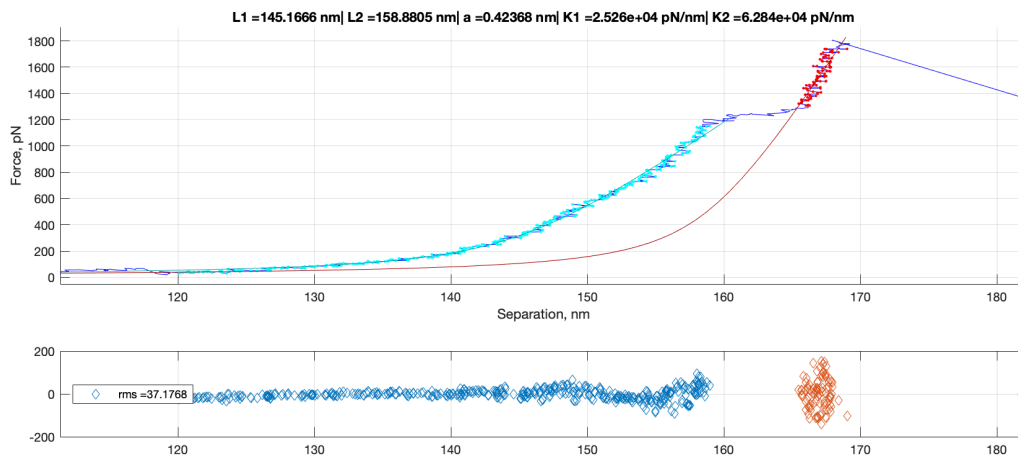


Figure S18: Representative FJC fitting of polymer P2b.

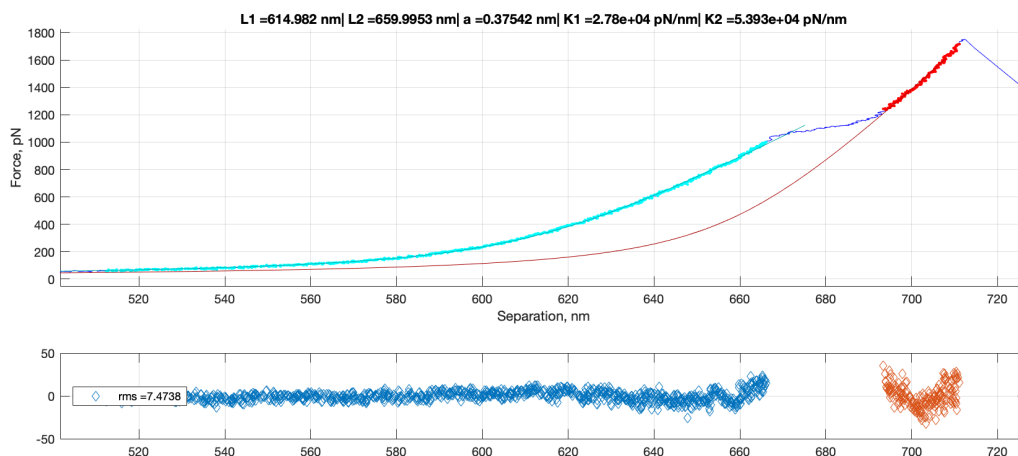


Figure S19: Representative FJC fitting of polymer P2c.

Obtaining the plateau force value, f^*

The characteristic plateau force, f^* , is defined here as the inflection point of the force-displacement curve (where derivative of the plateau of the force-displacement curve changes sign), and it can be mathematically defined as the x-intercept of the plot of the second derivative of the force vs. displacement curve. Plateau force values were obtained here via Matlab.

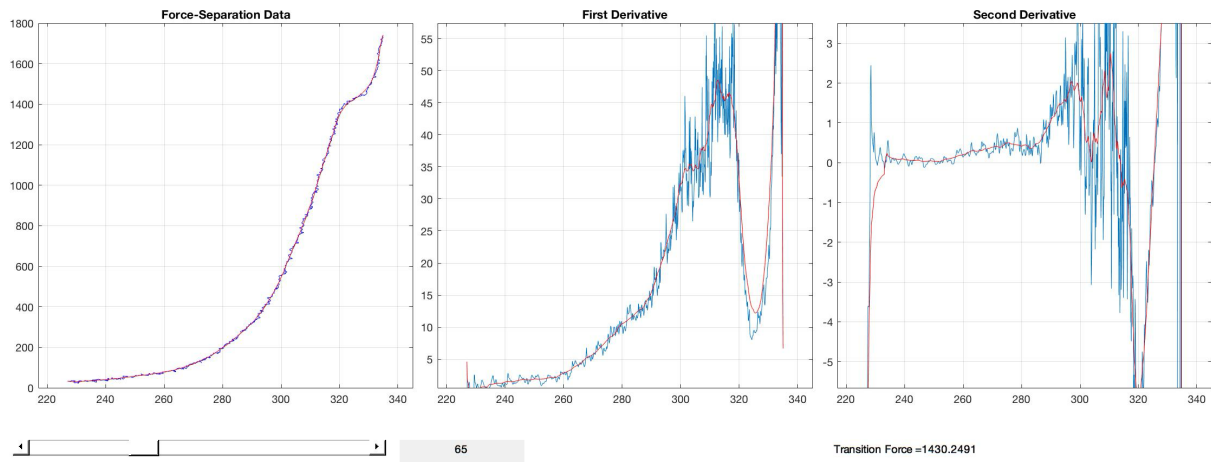


Figure S20: Representative force curve with f^* analysis for polymer P2a.

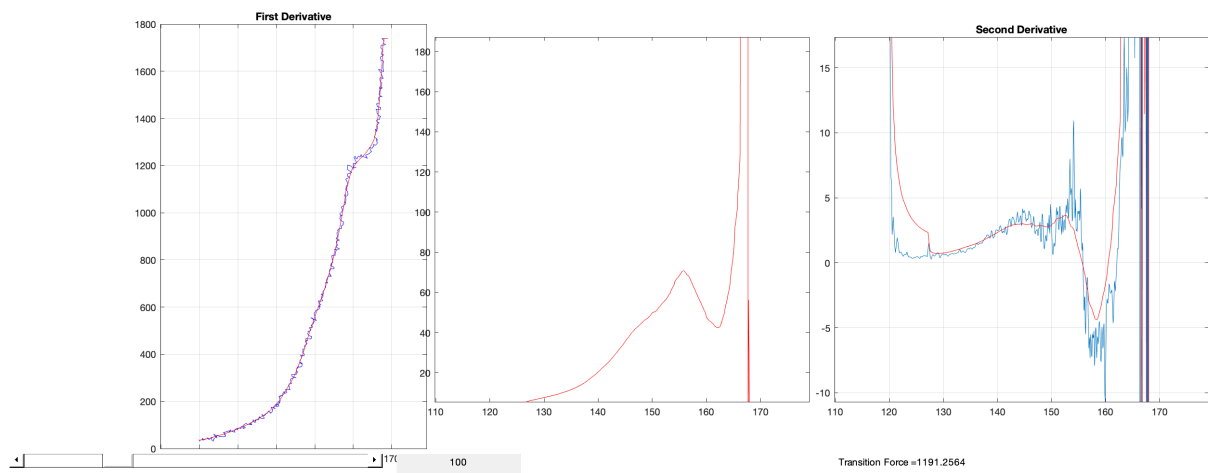


Figure S21: Representative force curve with f^* analysis for polymer P2b.

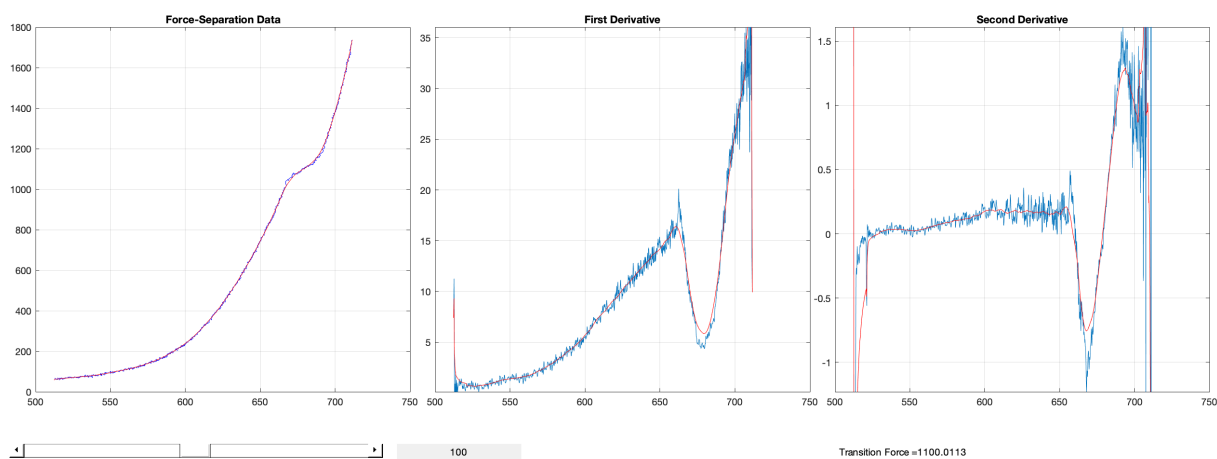


Figure S22: Representative force curve with f^* analysis for polymer P2c.

Table S2. Calculated and observed strand extensions for **P1b**.

Polymer	%CBE	$L2/L1$ (FJC)	$L2/L1$ (Modelin g-EE)	$L2/L1$ (Modelin g-EZ)	f^* (pN)
P1b	0.16	1.08	1.06	1.04	1671
P1b	0.16	1.09	1.06	1.04	1655
P1b	0.16	1.08	1.06	1.04	1660
P1b	0.16	1.09	1.06	1.04	1655
P1b	0.16	1.05	1.06	1.04	1635
P1b	0.16	1.05	1.06	1.04	1602
P1b	0.16	1.04	1.06	1.04	1547
P1b	0.16	1.10	1.06	1.04	1451
P1b	0.16	1.07	1.06	1.04	1505
P1b	0.16	1.04	1.06	1.04	1489
AVG		1.07			1580
		±0.02			±80

Table S3. Calculated and observed strand extensions for **P1c**.

Polymer	%CBE	<i>L2/L1</i> (FJC)	<i>L2/L1</i> (Modelin g-EE)	<i>L2/L1</i> (Modelin g-EZ)	<i>f</i> * (pN)
P1c	0.18	1.08	1.06	1.04	1419
P1c	0.18	1.07	1.06	1.04	1470
P1c	0.16	1.08	1.06	1.04	1388
P1c	0.16	1.08	1.06	1.04	1445
P1c	0.16	1.11	1.06	1.04	1383
P1c	0.16	1.06	1.06	1.04	1475
P1c	0.16	1.08	1.06	1.04	1475
P1c	0.16	1.10	1.06	1.04	1472
AVG		1.08			1440
		±0.02			±20

Table S4. Calculated and observed strand extensions for **P2a**.

Polymer	%CBE	<i>L2/L1</i> (FJC)	<i>L2/L1</i> (Modelin g-EE)	<i>L2/L1</i> (Modelin g-EZ)	<i>f</i> * (pN)
P2a	0.17	1.06	1.06	1.04	1430
P2a	0.17	1.09	1.06	1.04	1433
P2a	0.17	1.07	1.06	1.04	1430
P2a	0.17	1.08	1.06	1.04	1380
P2a	0.17	1.07	1.06	1.04	1430
P2a	0.17	1.06	1.06	1.04	1434
AVG		1.07			1421
		±0.01			±20

Table S5. Calculated and observed strand extensions for **P2b**.

Polymer	%CBE	<i>L2/L1</i> (FJC)	<i>L2/L1</i> (Modelin g-EE)	<i>L2/L1</i> (Modelin g-EZ)	<i>f</i> * (pN)
P2b	0.13	1.08	1.05	1.04	1219

P2b	0.13	1.06	1.05	1.04	1309
P2b	0.13	1.09	1.05	1.04	1191
P2b	0.13	1.07	1.05	1.04	1288
P2b	0.13	1.10	1.05	1.04	1204
AVG		1.08			1242
		±0.02			±53

Table S6. Calculated and observed strand extensions for **P2c**.

Polymer	%CBE	<i>L2/L1</i> (FJC)	<i>L2/L1</i> (Modelin g-EE)	<i>L2/L1</i> (Modelin g-EZ)	<i>L2/L1</i> (Modelin g-ZE)	<i>f*</i> (pN)
P2c	0.17	1.09	1.08	1.06	1.06	1092
P2c	0.17	1.07	1.08	1.06	1.06	1100
P2c	0.17	1.07	1.08	1.06	1.06	1036
P2c	0.17	1.10	1.08	1.06	1.06	1110
P2c	0.17	1.11	1.08	1.06	1.06	1104
P2c	0.17	1.06	1.08	1.06	1.06	1107
P2c	0.17	1.07	1.08	1.06	1.06	1015
P2c	0.17	1.08	1.08	1.06	1.06	1083
P2c	0.17	1.08	1.08	1.06	1.06	1085
P2c	0.17	1.08	1.08	1.06	1.06	1073
P2c	0.17	1.07	1.08	1.06	1.06	1116
P2c	0.17	1.11	1.08	1.06	1.06	1126
P2c	0.17	1.10	1.08	1.06	1.06	1112
AVG		1.08				1089
		±0.02				±32

Mechanical Activation by Pulsed Ultrasonication

General Sonication Conditions.

A solution of 20 mg of polymer in 20 mL THF was transferred to a Suslick vessel and the solution was bubbled with nitrogen for 30 minutes before sonication. An aliquot was taken directly before sonication and analyzed by GPC-MALS-UV-Vis. The solution was sonicated under N₂ in an ice water bath (~6-9 °C) at 8.7 W/cm² with a pulse sequence of 1 sec. on 1 sec. off. The total 'pulse on' time was 1 hour. Another aliquot was taken directly after sonication and analyzed by GPC-MALS-UV-Vis. H¹ NMR of the post-sonicated solutions reveal that mechanical activation of the CBE mechanophores generates the thermally forbidden disrotatory ring-opened products.

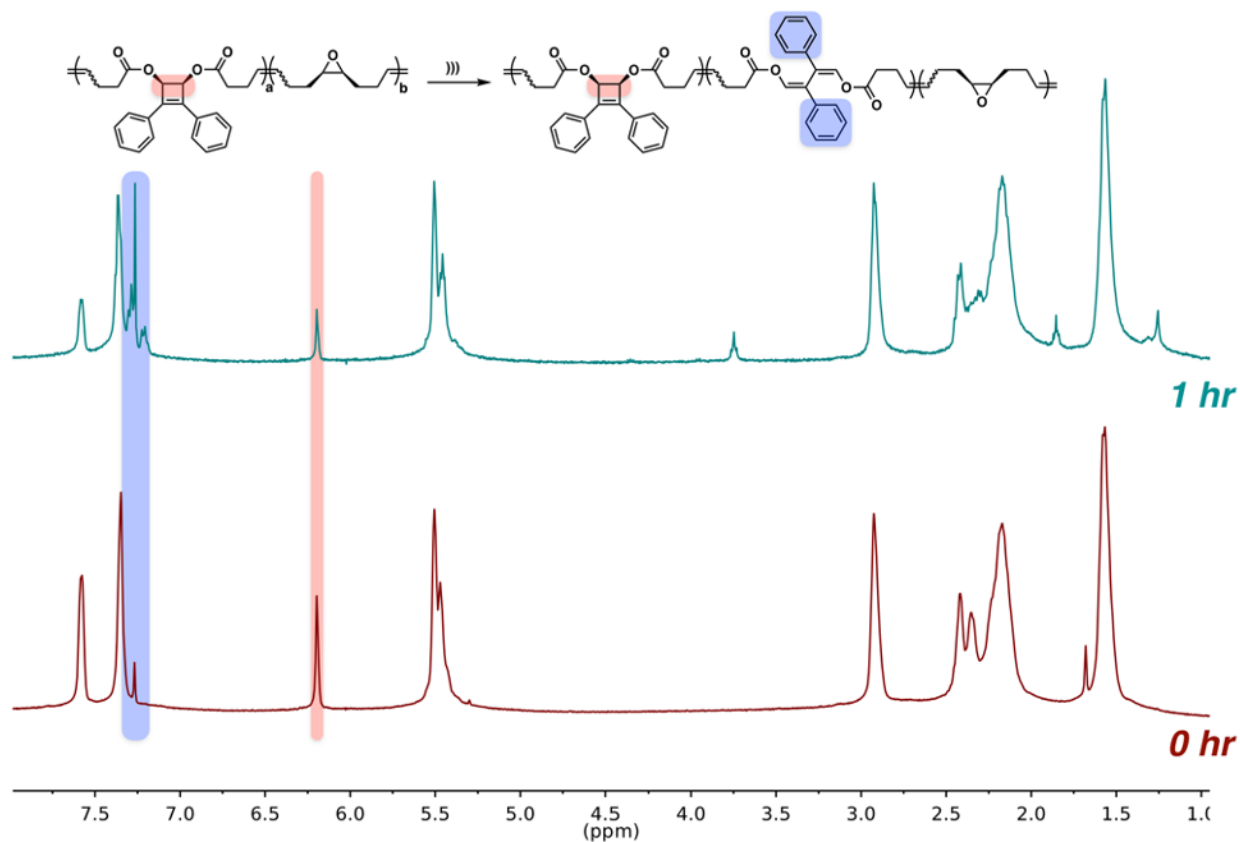


Figure S23. NMR spectra of **P1a** before and after sonication.

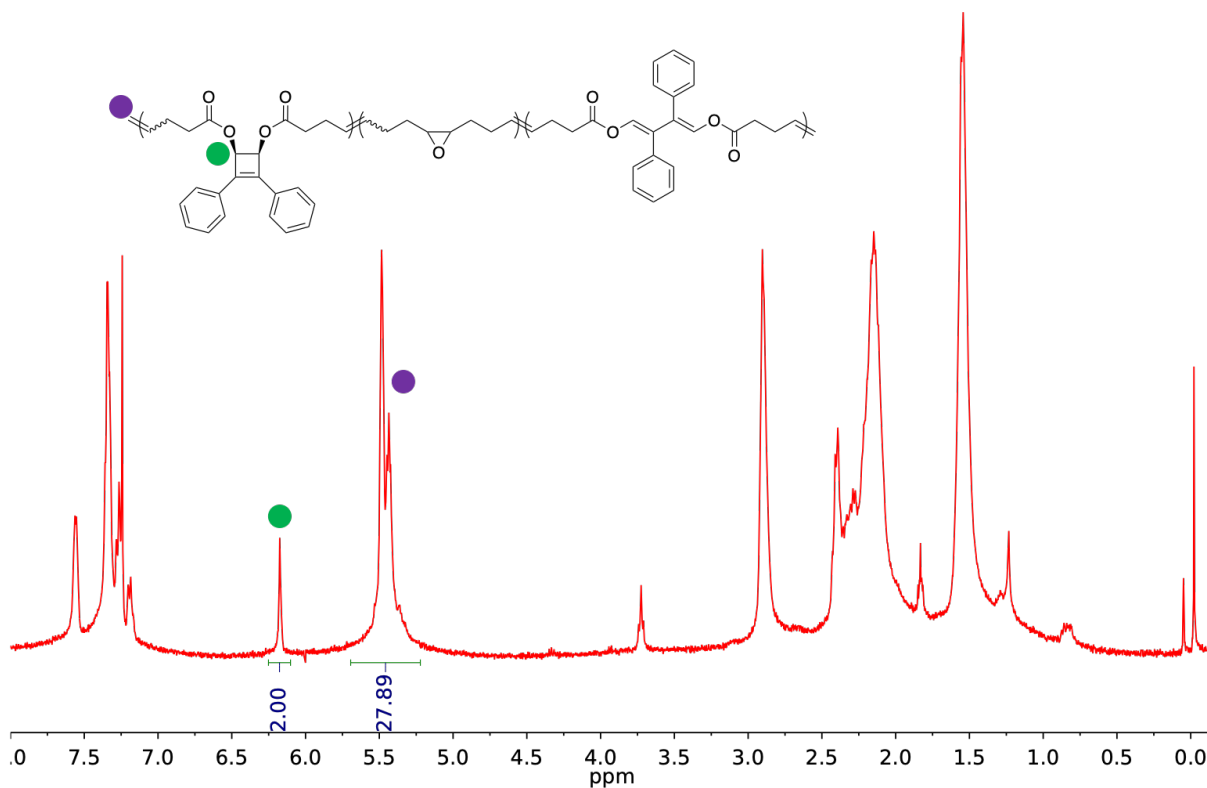


Figure S24. Post-sonication peaks chosen for analysis of mechanophore activation in **P1a**. The percent mechanophore activation was calculated by comparing the % intact CBEs after sonication and the % CBE in the nascent polymer. Percent intact CBE post-sonication = green/purple x 100% = 2.00 / 27.89 x 100% = 7%. Percent CBE pre-sonication = 19%. The percent mechanophore activation = (19-7) / 19 x 100% = 63%. SECS-MALS: Pre-sonication: Mn = 75.3 kD, Mw = 121 kD, D = 1.6. Post-sonication: Mn = 30 kD, Mw = 38 kD, D = 1.2.

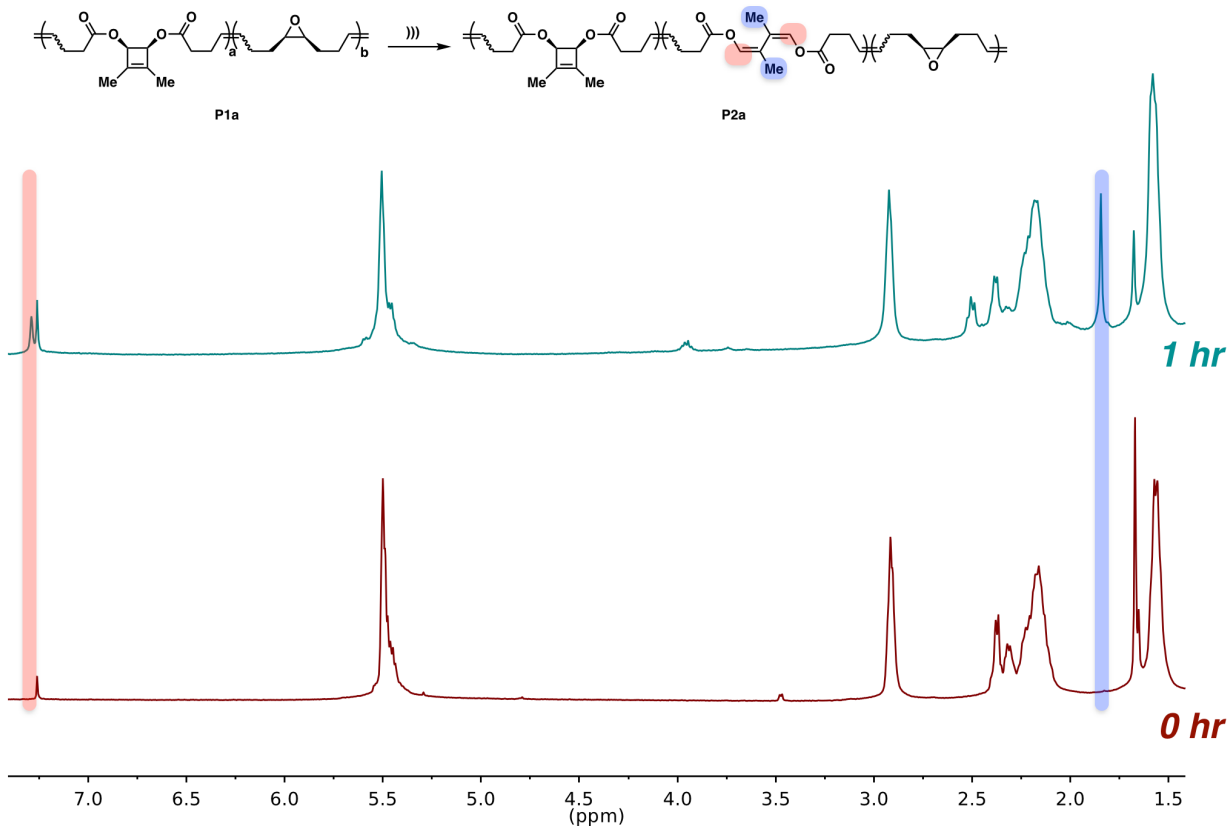


Figure S25. NMR spectra of **P2a** before and after sonication. Integration gives 65% mechanophore activation.

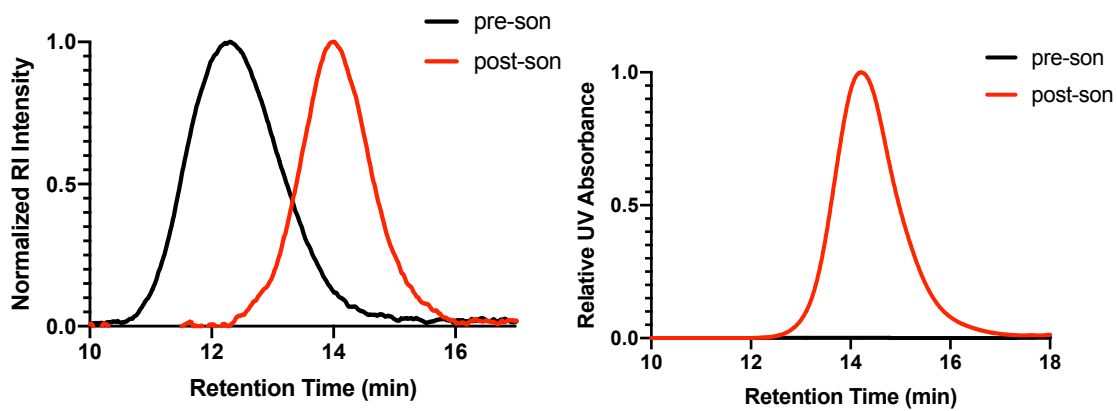


Figure S26. SEC of **P2a** before and after sonication. Mn: 82→21 (Mw = 31, D = 1.5)

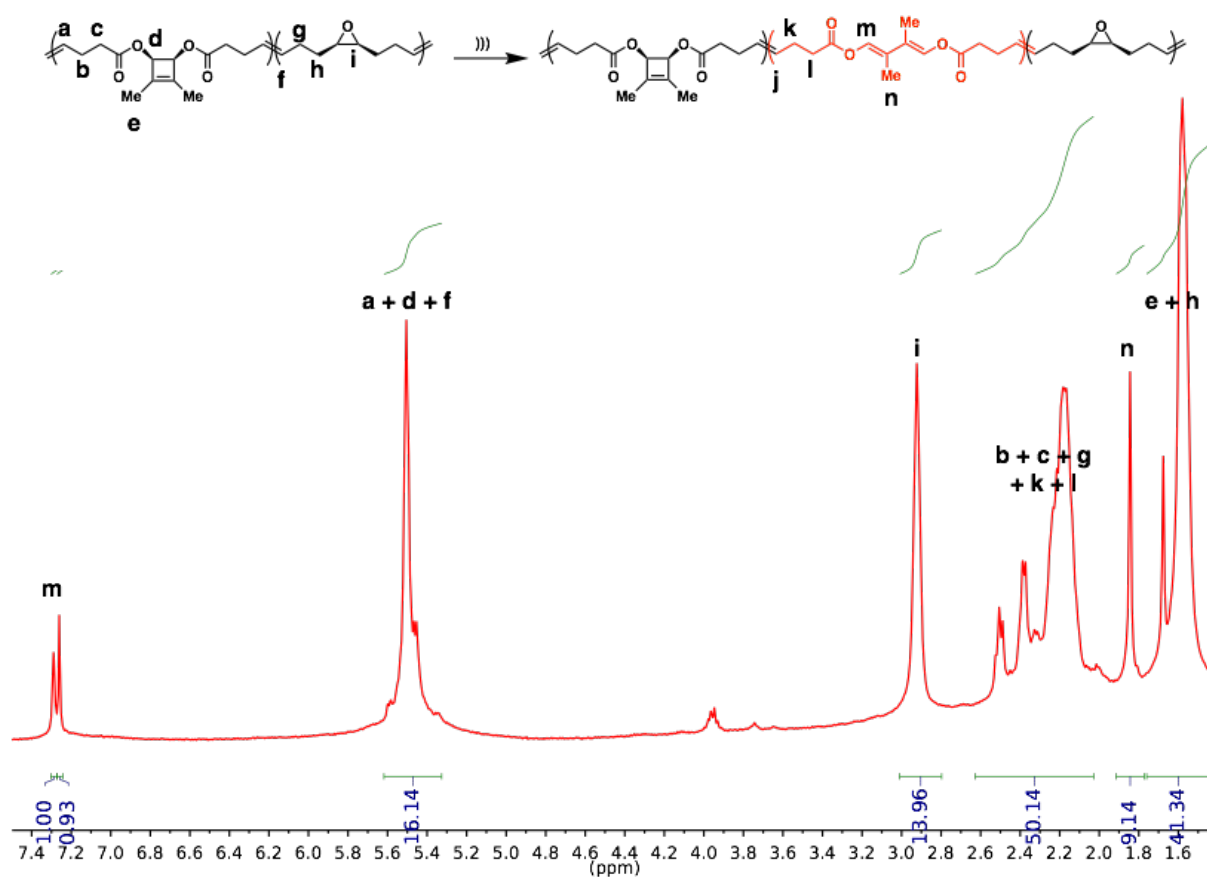


Figure S27: Calculation of percent mechanophore activation in polymer **P2a**. The integration of i was compared to the combined integration of a, d, and f because these regions in the spectrum are unchanged from the pre-sonicated spectrum, aside from decreased signal from d due to CBE ring opening. Applying the same calculation as above, percent non-activated cyclobutene = 7.0%. Therefore, percent activated mechanophore = $(19.8 - 7.0) / 19.8 \times 100\% = 65\%$.

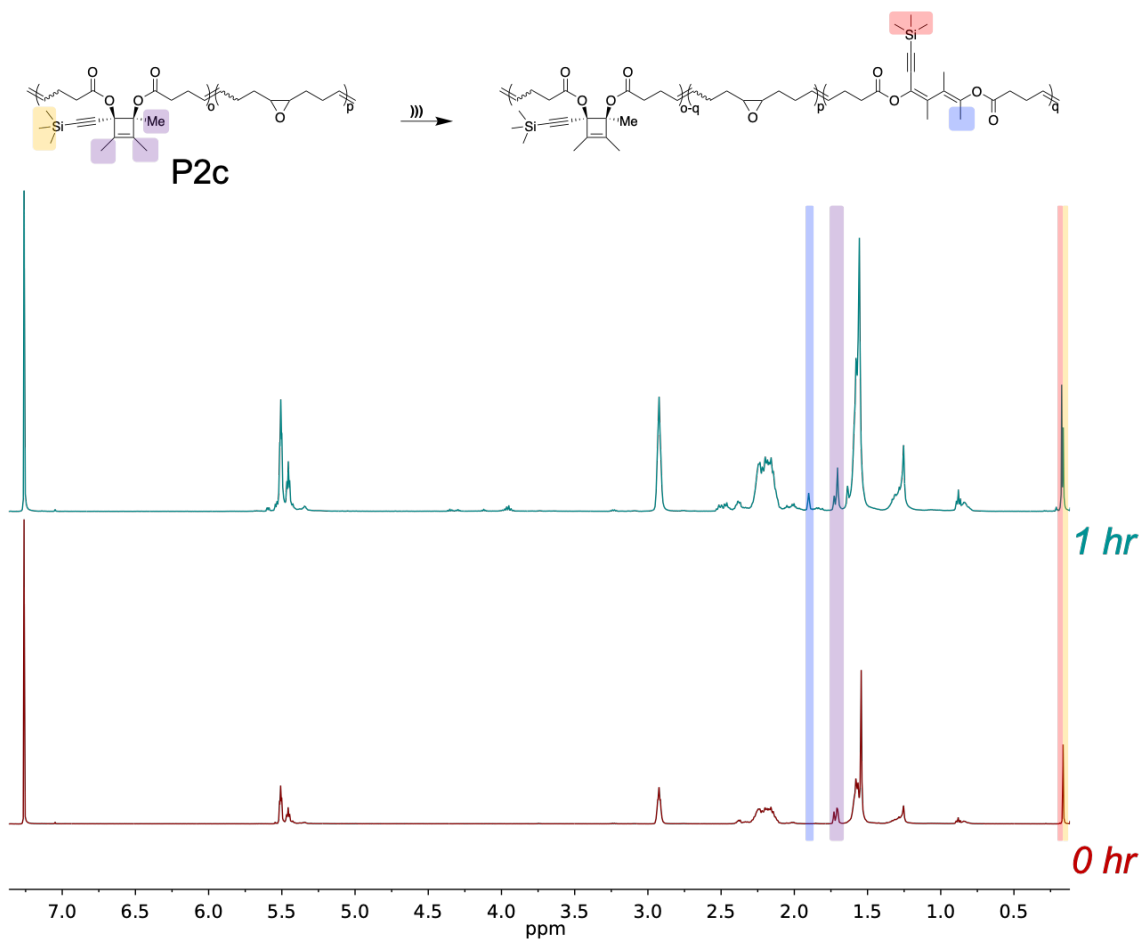


Figure S28. NMR spectra of P2c before and after sonication.

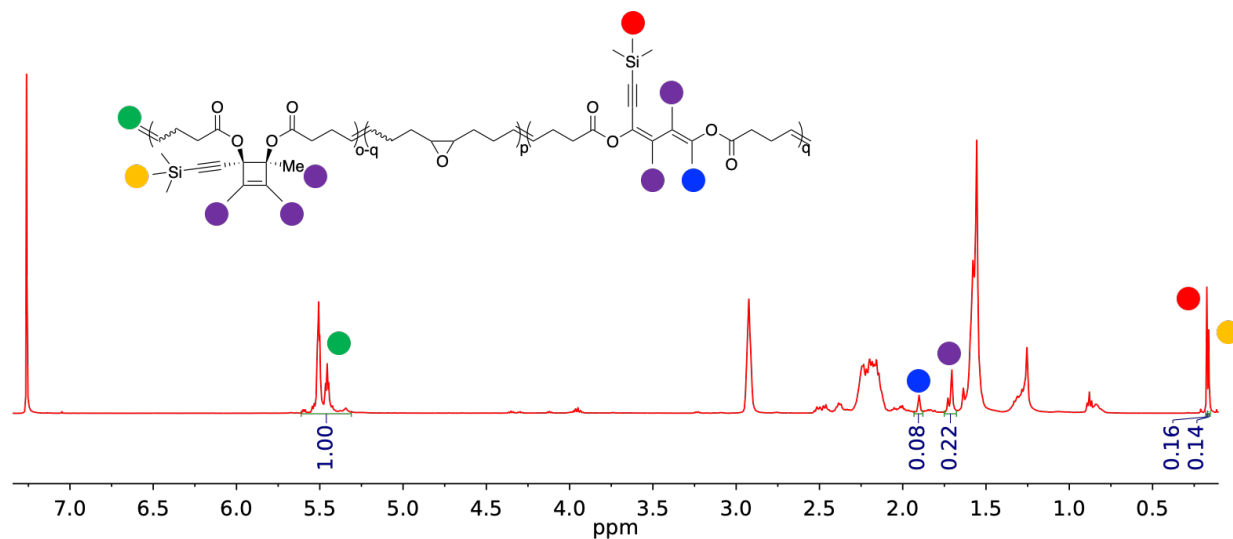


Figure S29: Calculation of percent mechanophore activation in polymer P2c. The percent activation can be calculated multiple ways. The easiest method is by directly

comparing post-sonicated-TMS to total TMS (pre- and post-sonication): $\text{red}/(\text{red}+\text{yellow}) \times 100\% = 0.16 / (0.16+0.14) \times 100\% = 53\%$.

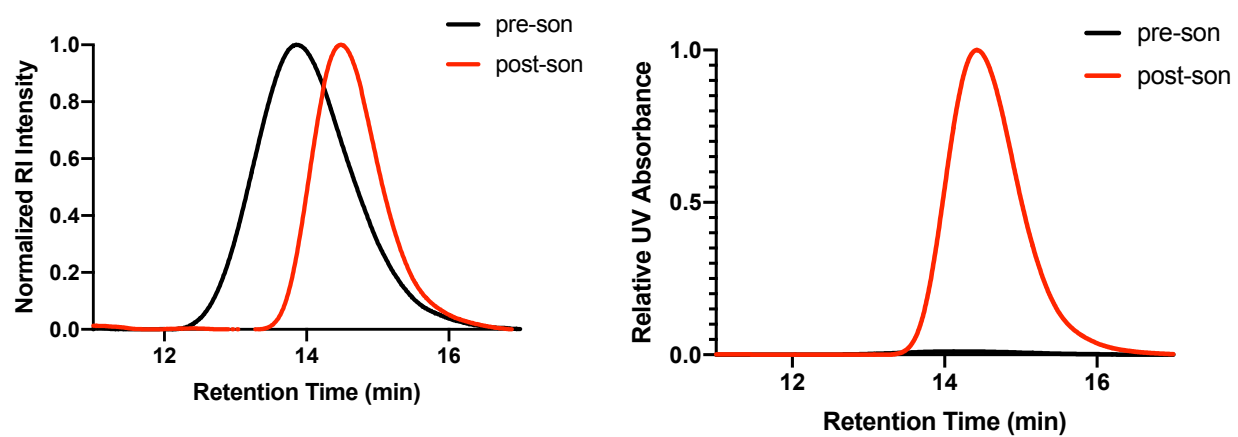


Figure S30. SEC of **P2c** before and after sonication. Mn: 56.1 → 28.1

FMPES Computations

The external mechanical force was described using a force-modified potential energy surface (FMPES).[14] This simulates the effect of a force that is constant on the time scale of molecular events. The external forces were applied to the two outermost carbon atoms of the model mechanophores. The effective potential is therefore modified by the term $-F_{ext} \cdot \Delta x$, which depends parametrically on the external force F :

$$V_{FMPES} = V_{el} - F_{ext} \cdot \Delta x$$

Here, Δx is the distance between the two atoms where the force is applied to. For the calculation of the electronic potential energy V_{el} , the B3LYP functional was used in combination with the 6-31G* basis set.[14-19] This combination has been evaluated in a previous study on related systems [20] showing that the energy landscapes are in good agreement with reference calculations based on complete active space perturbation theory (CASPT2).

Graphical Processing units (GPUs) have been used to accelerate the calculation of the electronic potential energy using the Terachem program package.[21, 22] The stationary points (minima and transition structures) were optimized using the DL-FIND optimization library[23] which was interfaced via Chemshell.[24] For the calculation of the free energy barriers, the reactants and transition state structures are optimized on the respective FMPES. Stationary points are verified by the correct number of imaginary eigenvalues of the Hessian matrix: none for minimum structures, and one for transition state structures. The rigid-rotor-harmonic-oscillator approximation has been used for the calculation of free energy barriers. Frequencies below 100 cm^{-1} are approximated by this value to avoid divergence of the entropic contribution for low-lying vibrational modes.

We want to mention that we found two distinct rotamers for the aryl substituted cis-CBEs, differing in the position of one aryl ring, see Figure S31. The two rotamers differ by at maximum 2.0 kcal/mol in energy, the right rotamer in Figure S31 being the energetically favorable one. The free energy barriers of these rotamers differ by at maximum 1.8 kcal/mol, around 1.0 kcal/mol on average. We are using the more stable rotamers (right in Figure S31) throughout.

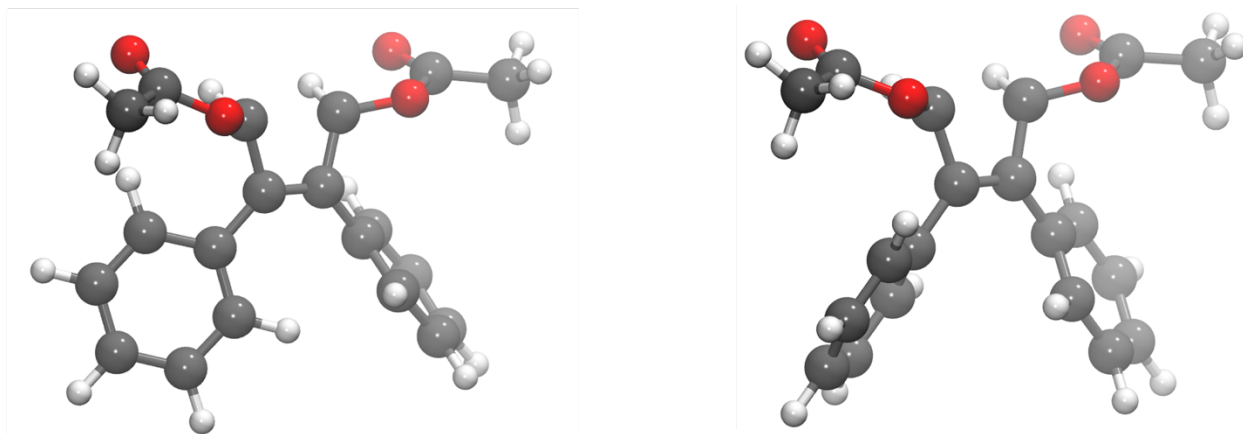


Figure S31: Transition structures of the two different rotamers of diphenyl-CBE. Left: The two phenyl rings have a higher steric repulsion and, thus, the structure is slightly higher in energy. This structure has also been used in our recent study.[7] Right: energetically more stable transition structure. The two phenyl rings are almost parallel, which reduces the steric repulsion.

The free energy barriers of the conrotatory (Woodward-Hoffmann allowed) ring-opening mechanism of the cis-substituted CBEs were calculated in 0.1 nN steps from 0.0 nN on. Higher pulling forces lead to a decrease in free energy barriers as intuitively expected. Above a system-dependent threshold force (see Tables S6 and S7), attempts to optimize the transition states associated with conrotatory ring-opening mechanisms converge to transition states associated with the disrotatory reaction mechanism. The free energy barriers of the disrotatory (Woodward-Hoffmann forbidden) ring-opening mechanism of the cis-substituted CBEs were calculated in 0.1 nN steps. Above a system-dependent critical force (see Tables S6 and S7), the reactant structure is not a stable minimum anymore and the ring-opening reaction would occur completely barrierless. On the other side, when the force is below a system dependent value (in most cases between 0.5 and 1.0 nN), attempts to optimize transition structures associated with the disrotatory mechanism failed, which is in accordance with studies by Sakai.[25]

Table S7: Barrier heights in kcal mol⁻¹ for disrotatory and conrotatory ring opening of compounds 1a-1c at different forces.

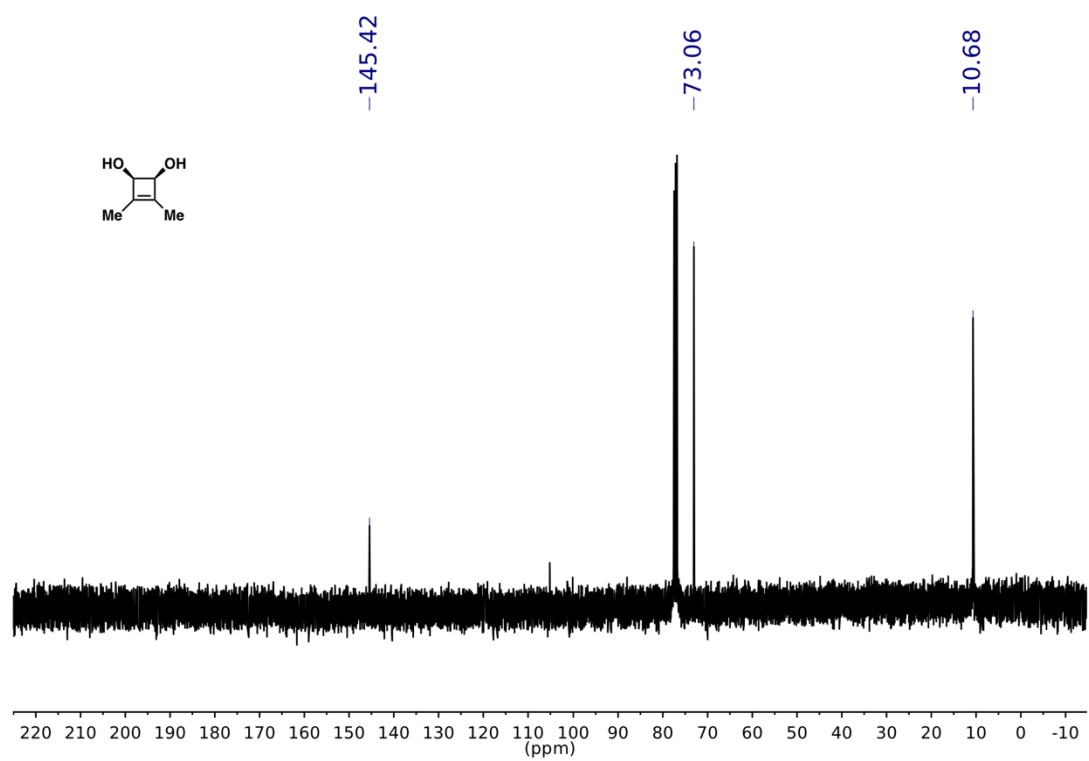
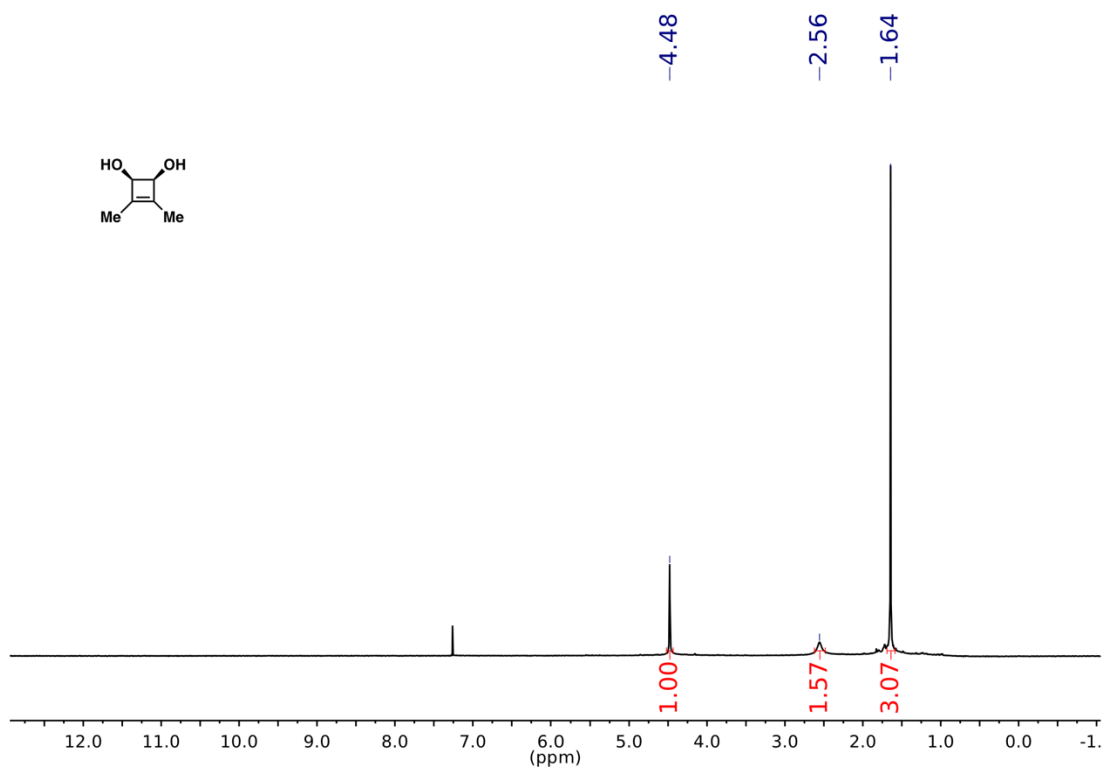
F/nN	1a: Disrot	1a: Conrot	1b: Disrot	1b: Conrot	1c: Disrot	1c: Conrot
0.0	---	31.74	---	30.65	---	33.65
0.1	---	32.65	---	32.16	---	32.11
0.2	---	32.28	---	32.31	---	30.89
0.3	---	31.23	---	31.82	---	29.75
0.4	---	30.30	---	31.13	---	28.57
0.5	---	29.28	---	29.86	---	27.70
0.6	---	27.33	---	28.44	---	26.68
0.7	---	26.70	---	27.09	---	25.92
0.8	31.42	25.97	---	25.94	---	25.45
0.9	28.76	24.75	---	24.67	28.73	24.38
1.0	26.57	23.61	---	23.62	26.67	23.39
1.1	24.39	22.39	---	22.30	24.79	22.47
1.2	22.46	21.27	22.94	20.86	22.97	21.38
1.3	20.74	19.49	20.99	19.66	21.21	20.40
1.4	19.23	18.60	19.20	18.29	19.66	19.25
1.5	17.61	17.48	17.63	17.07	19.06	18.92
1.6	16.08	16.25	16.03	15.42	16.63	17.16
1.7	14.65	15.17	14.62	14.21	15.28	15.74
1.8	13.34	14.09	13.20	13.15	13.55	14.02
1.9	12.11	13.03	11.88	11.93	12.32	13.02
2.0	11.09	12.11	10.59	11.10	11.12	11.73
2.1	9.71	10.79	9.26	9.76	9.94	10.80
2.2	8.62	9.55	8.12	8.59	8.86	10.30
2.3	7.59	8.33	7.02	7.32	7.70	9.02
2.4	6.63	7.06	6.09	6.09	6.81	8.29
2.5	5.71	5.85	5.07	4.95	5.75	7.22
2.6	4.86	4.66	4.32	3.96	5.19	6.62
2.7	4.09	3.64	3.47	3.06	4.35	5.64
2.8	3.26	2.52	2.66	---	3.64	---
2.9	2.67	1.52	1.89	---	2.85	---
3.0	2.05	0.35	1.24	---	2.19	---
3.1	1.43	0.27	0.59	---	2.04	---
3.2	1.52	---	0.60	---	1.72	---
3.3	1.35	---	0.29	---	1.55	---
3.4	1.39	---	-0.03	---	1.40	---
3.5	1.60	---	0.30	---	---	---

Table S8: Barrier heights in kcal mol⁻¹ for disrotatory and conrotatory ring opening of compounds 2a-2c at different forces.

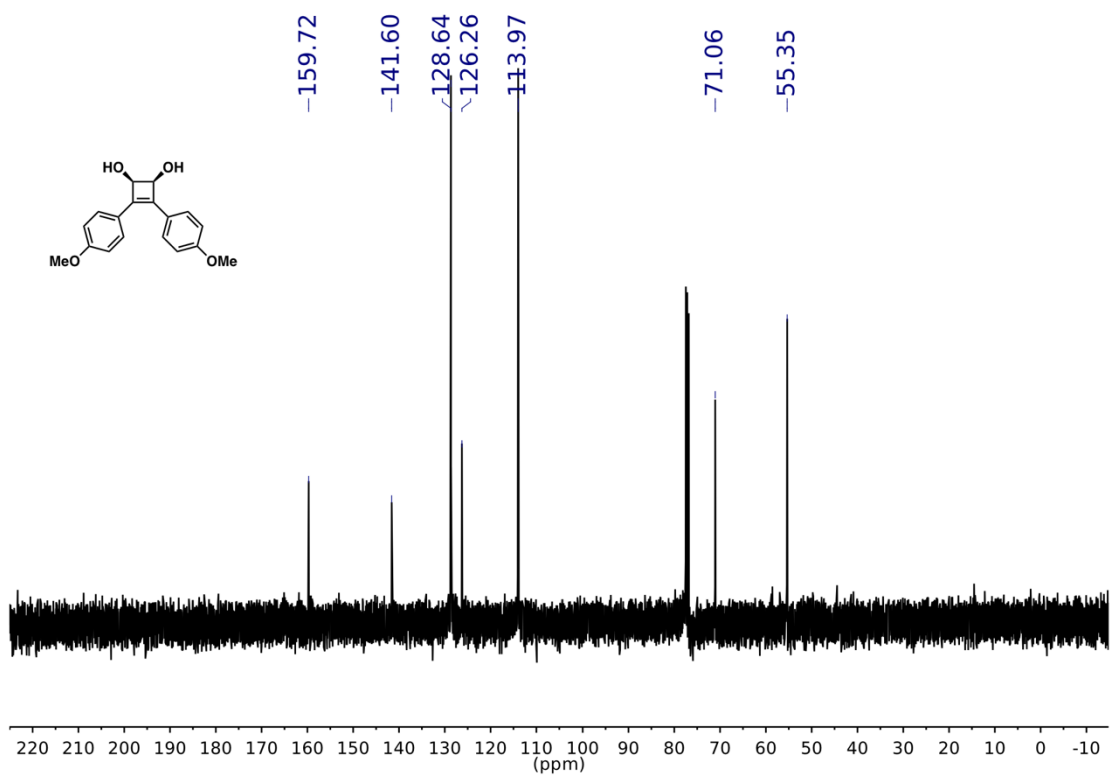
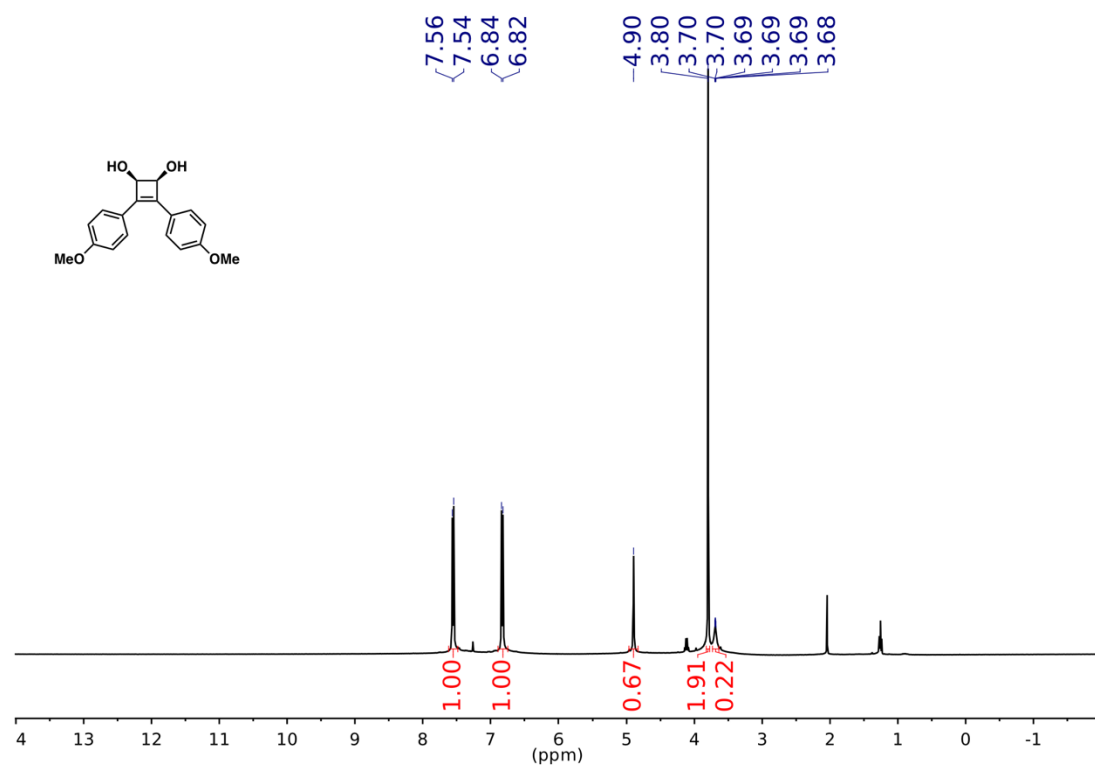
F/nN	2a: Disrot	2a: Conrot	2b: Disrot	2b: Conrot	2c: Disrot	2c: Conrot
0.0	---	33.90	---	38.17	---	38.56
0.1	---	35.67	---	37.99	---	35.97
0.2	---	35.61	---	36.15	---	33.17
0.3	---	35.04	---	35.95	33.94	30.47
0.4	40.11	34.75	---	34.49	31.01	27.93
0.5	37.20	33.68	---	34.11	28.00	24.92
0.6	34.37	32.45	33.12	32.77	25.18	22.91
0.7	31.72	30.97	29.99	30.59	22.66	21.00
0.8	29.29	29.16	26.76	28.52	20.37	19.12
0.9	26.97	27.66	23.93	26.58	18.10	17.32
1.0	24.74	26.43	22.01	24.92	15.88	15.79
1.1	22.84	25.24	19.42	22.92	14.11	14.40
1.2	20.87	23.83	17.08	20.74	12.12	12.92
1.3	19.37	22.79	15.02	18.77	10.34	11.53
1.4	17.72	21.52	13.29	16.93	8.60	10.28
1.5	16.11	20.05	11.18	14.88	7.15	9.37
1.6	14.49	18.61	9.39	12.60	5.56	8.29
1.7	13.06	17.18	7.80	10.88	4.35	7.32
1.8	11.93	16.11	6.24	8.80	3.04	6.18
1.9	10.27	14.19	5.27	7.34	2.16	4.96
2.0	9.13	12.96	3.89	5.55	0.89	3.89
2.1	7.94	11.26	2.60	3.33	0.16	2.94
2.2	6.84	9.72	1.42	1.27	-0.28	2.27
2.3	5.83	8.42	0.35	---	-0.69	---
2.4	4.84	6.98	---	---	---	---
2.5	3.92	6.39	---	---	---	---
2.6	3.05	---	---	---	---	---
2.7	2.41	---	---	---	---	---
2.8	1.69	---	---	---	---	---
2.9	1.03	---	---	---	---	---
3.0	1.10	---	---	---	---	---
3.1	0.81	---	---	---	---	---
3.2	0.73	---	---	---	---	---

NMR Spectra

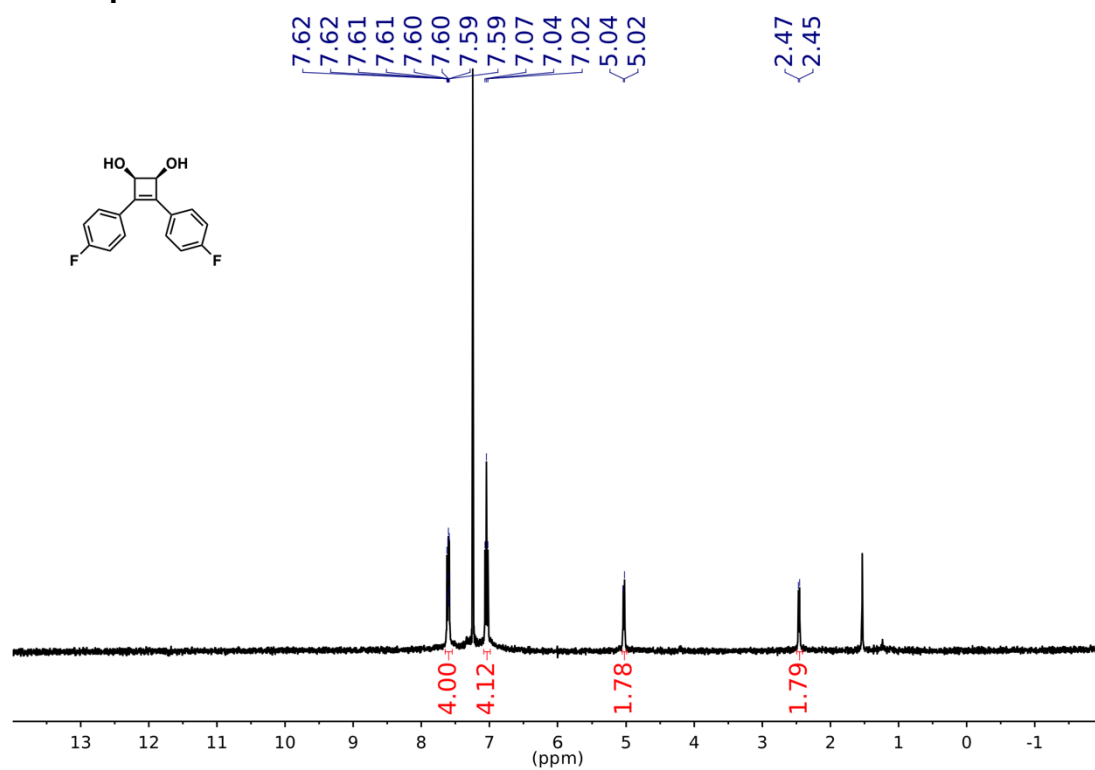
NMR Spectra of 2a-diol



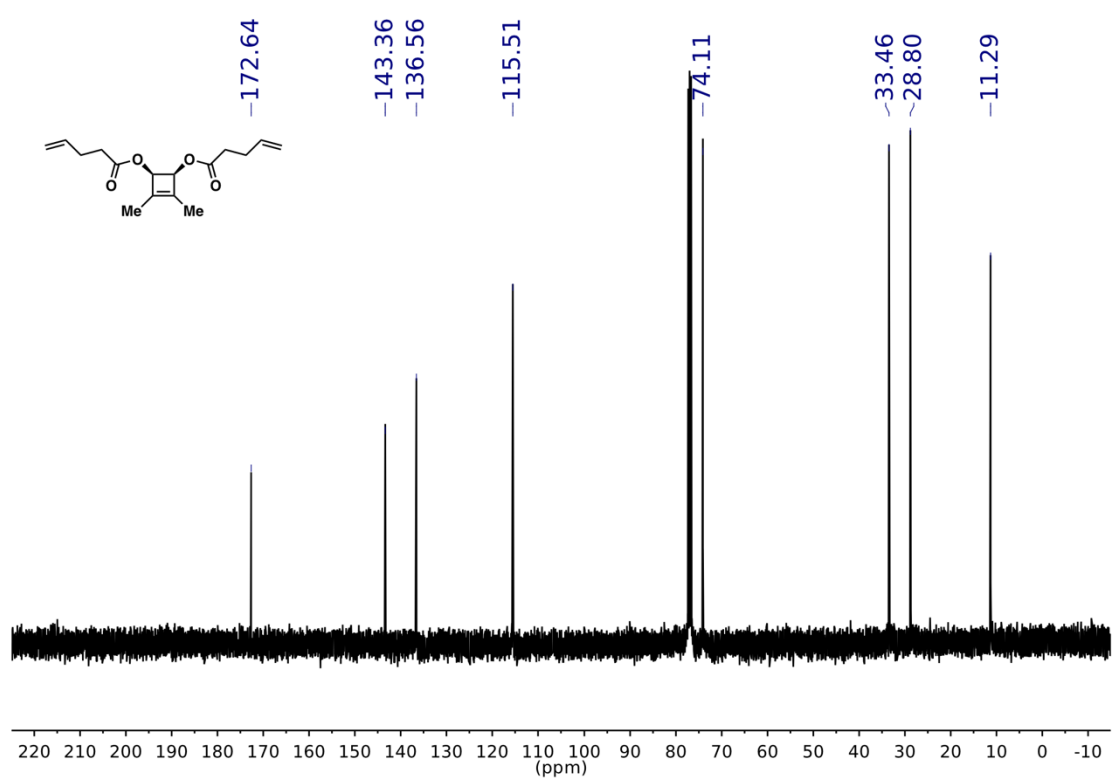
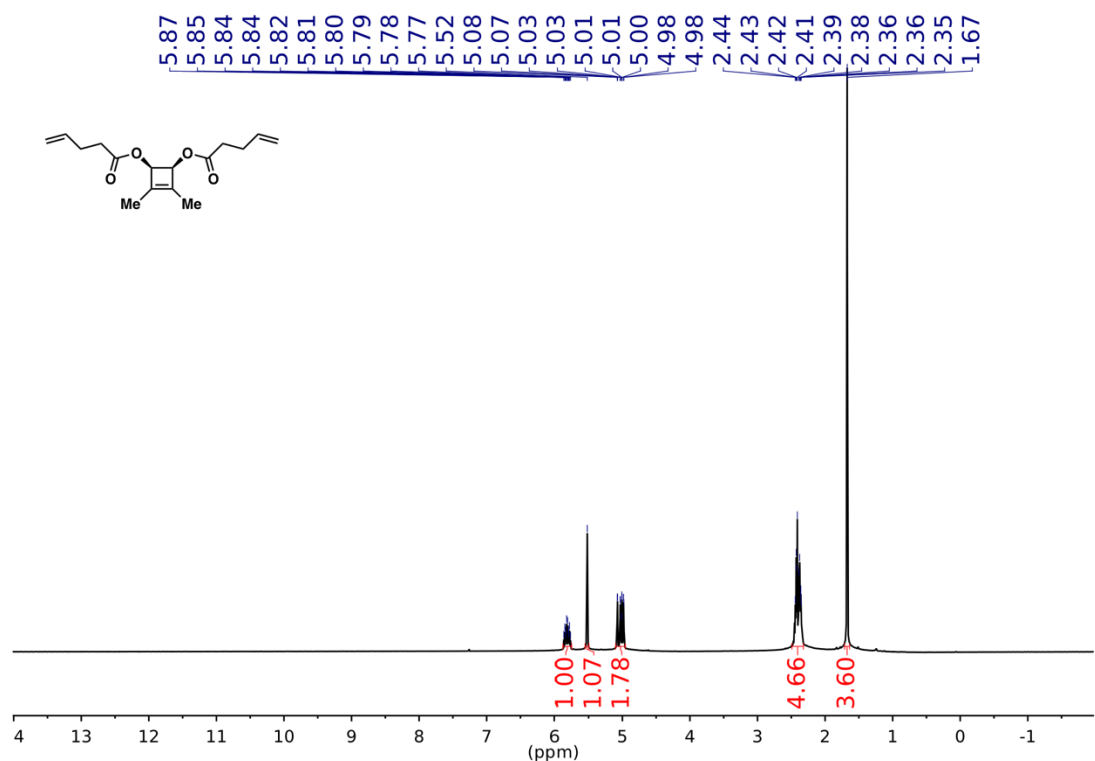
NMR Spectra of 1c-diol



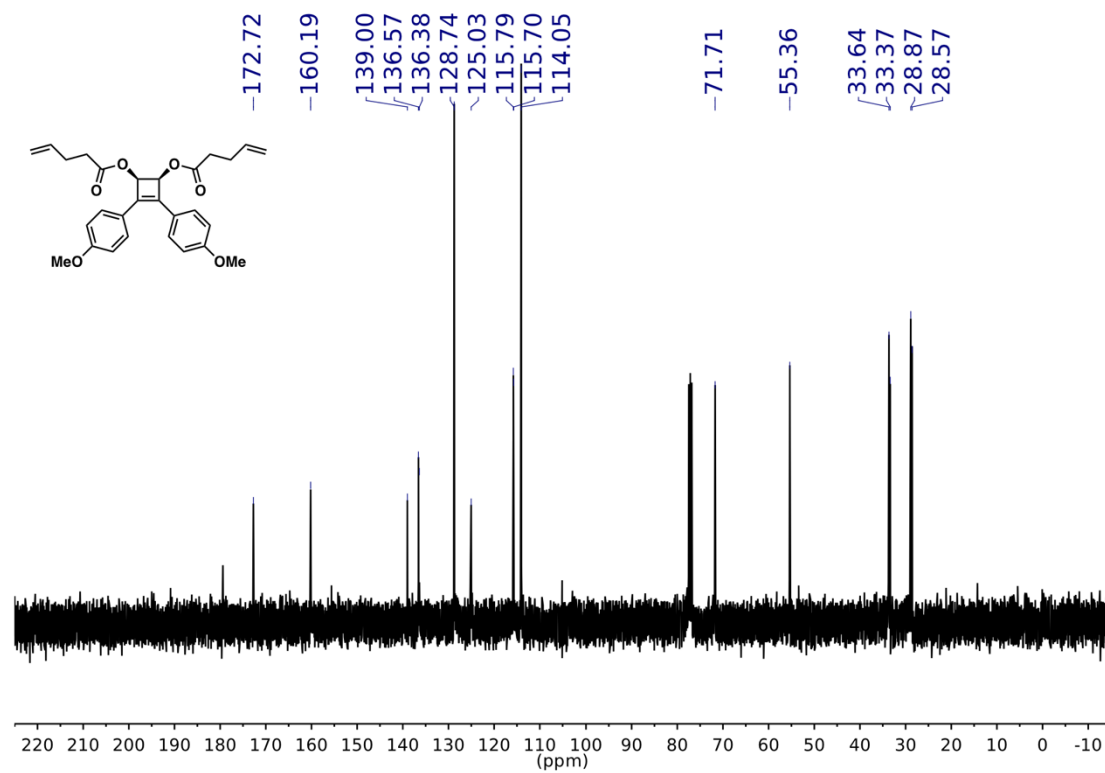
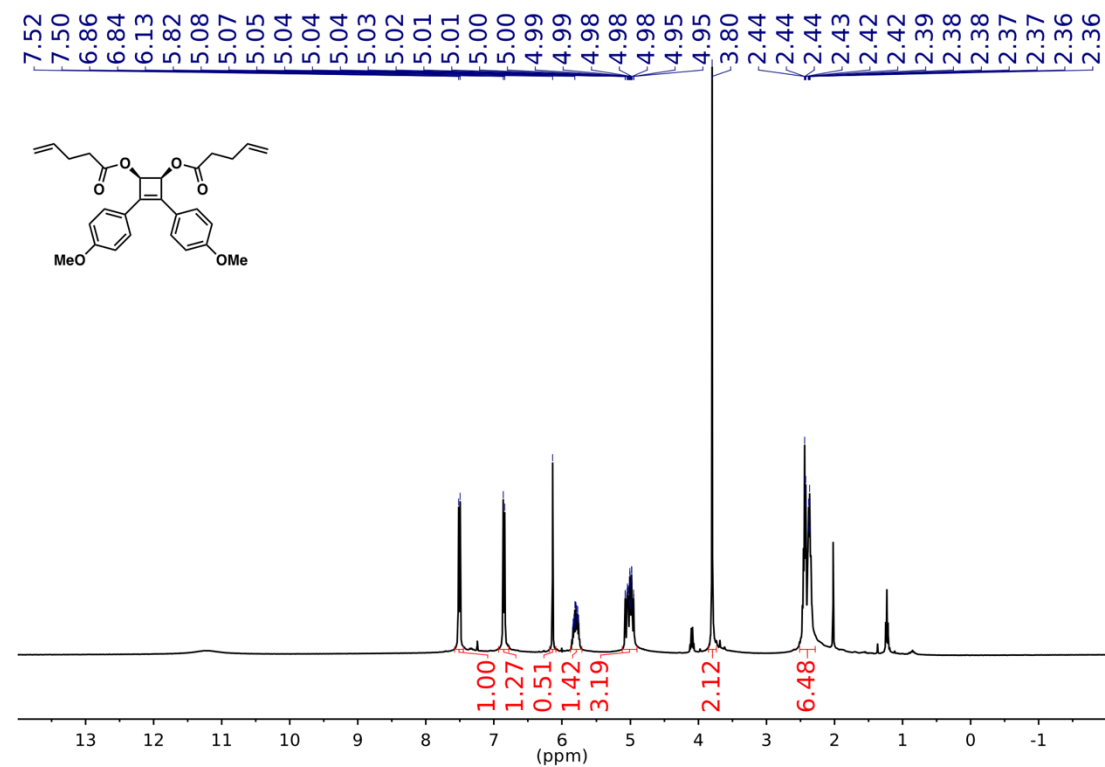
NMR Spectrum of 1c-diol



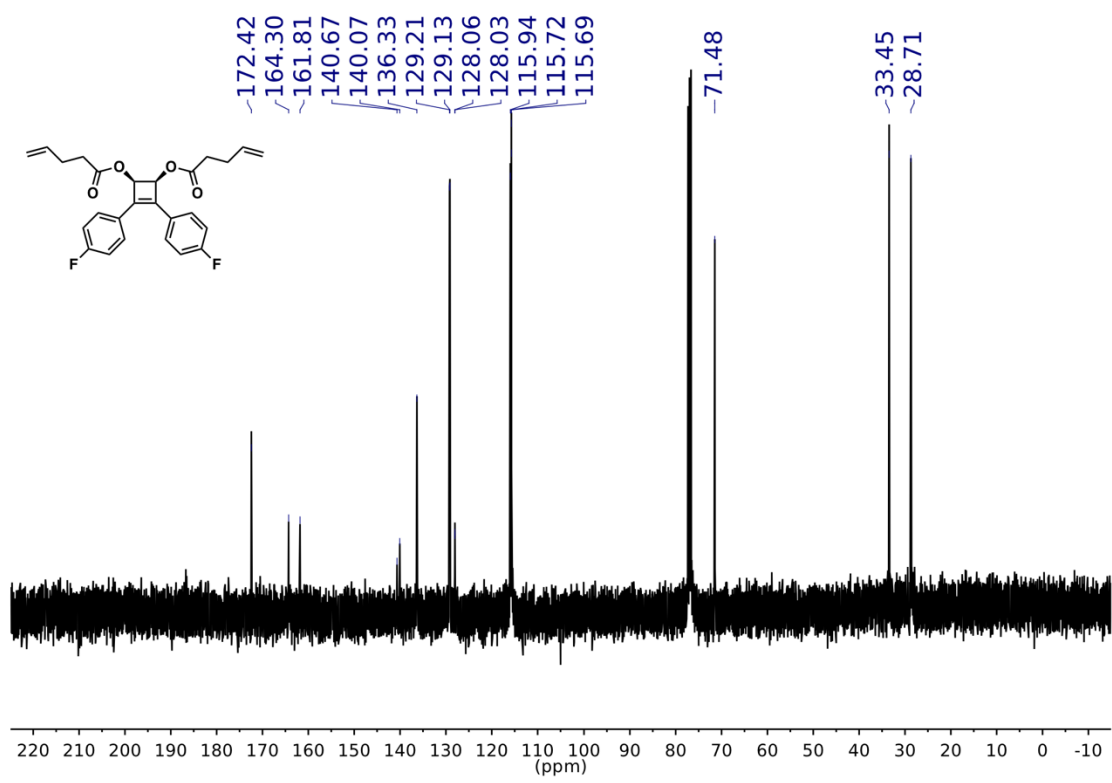
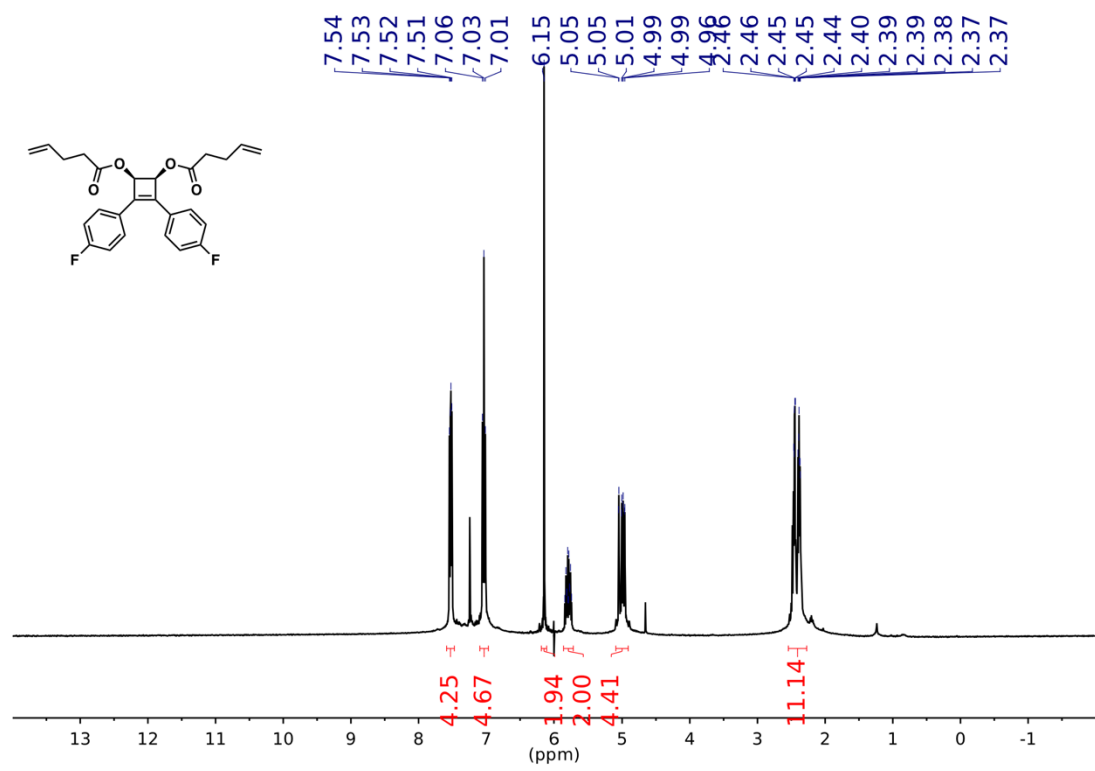
NMR Spectra of 2a-bisalkene



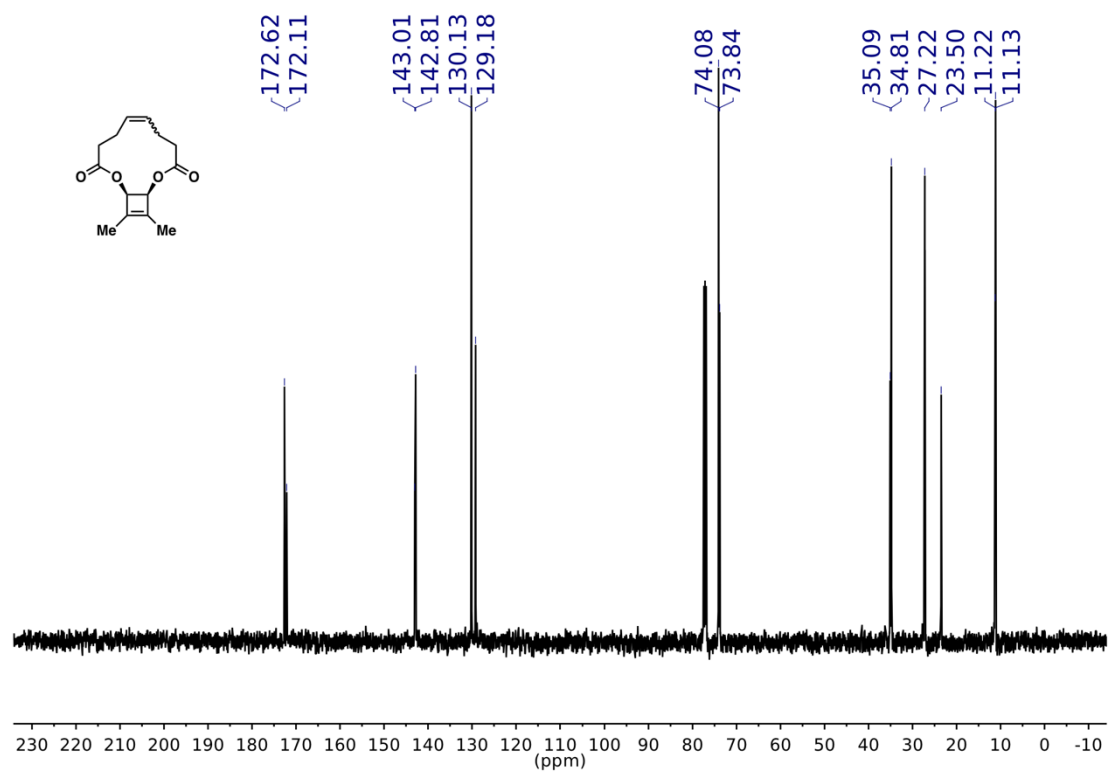
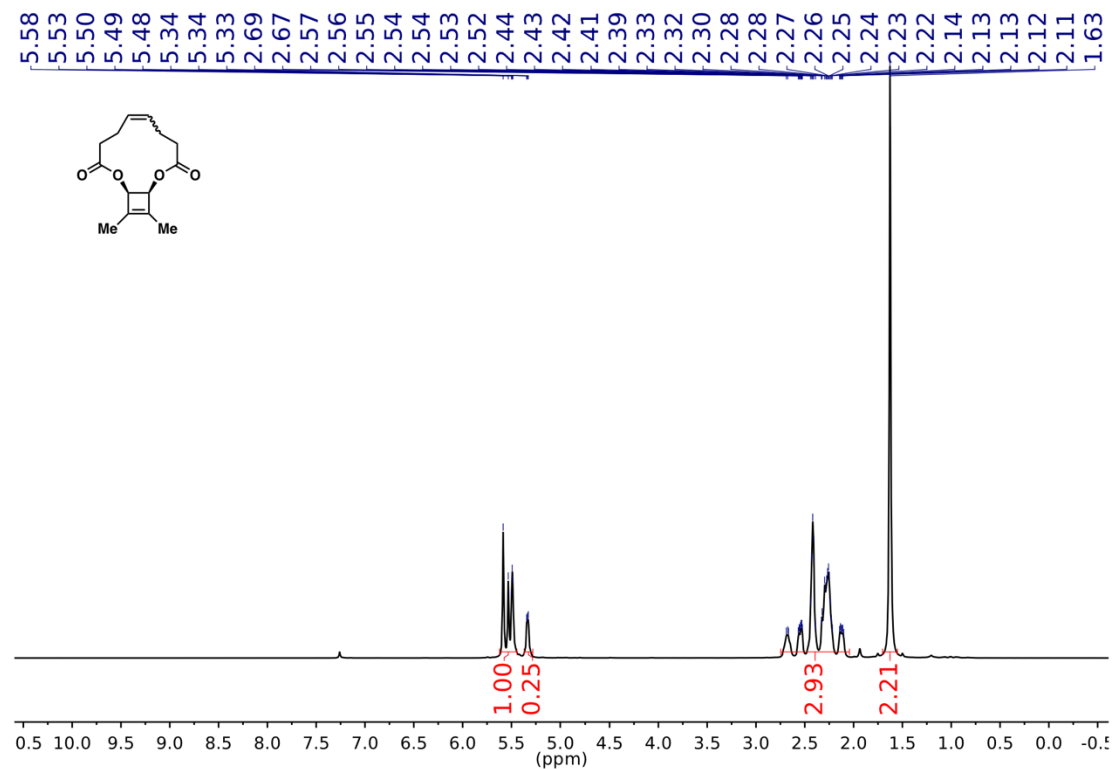
NMR Spectra of 1b-bisalkene



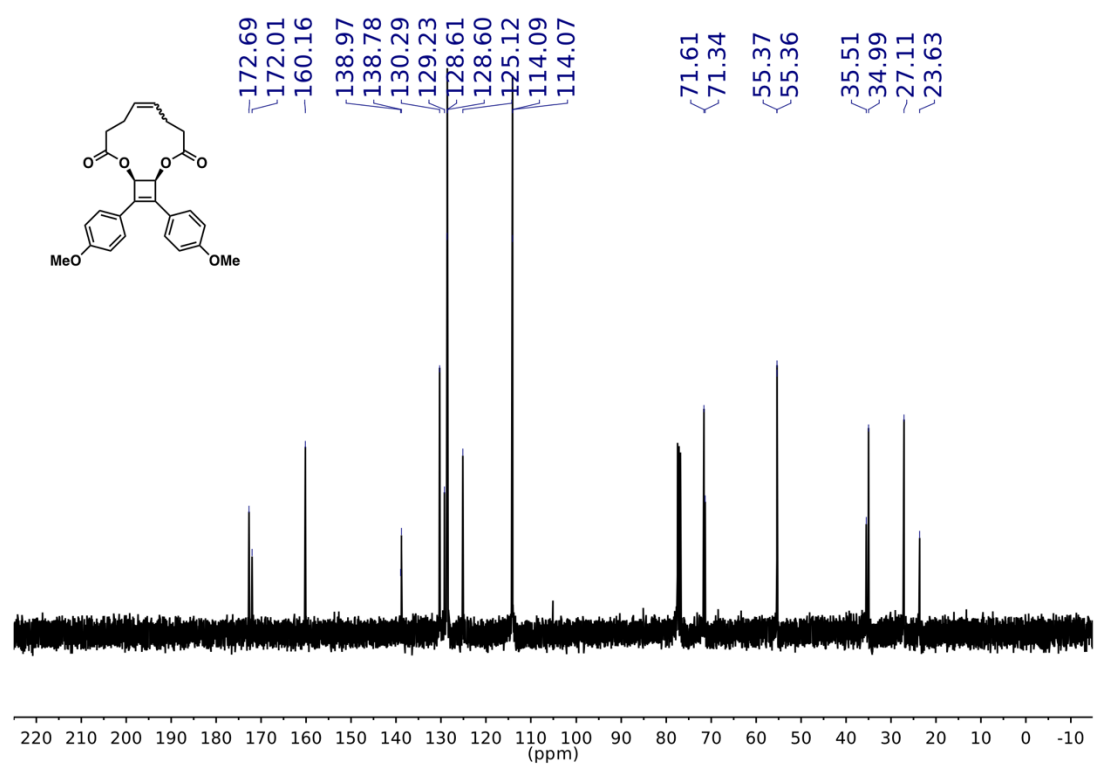
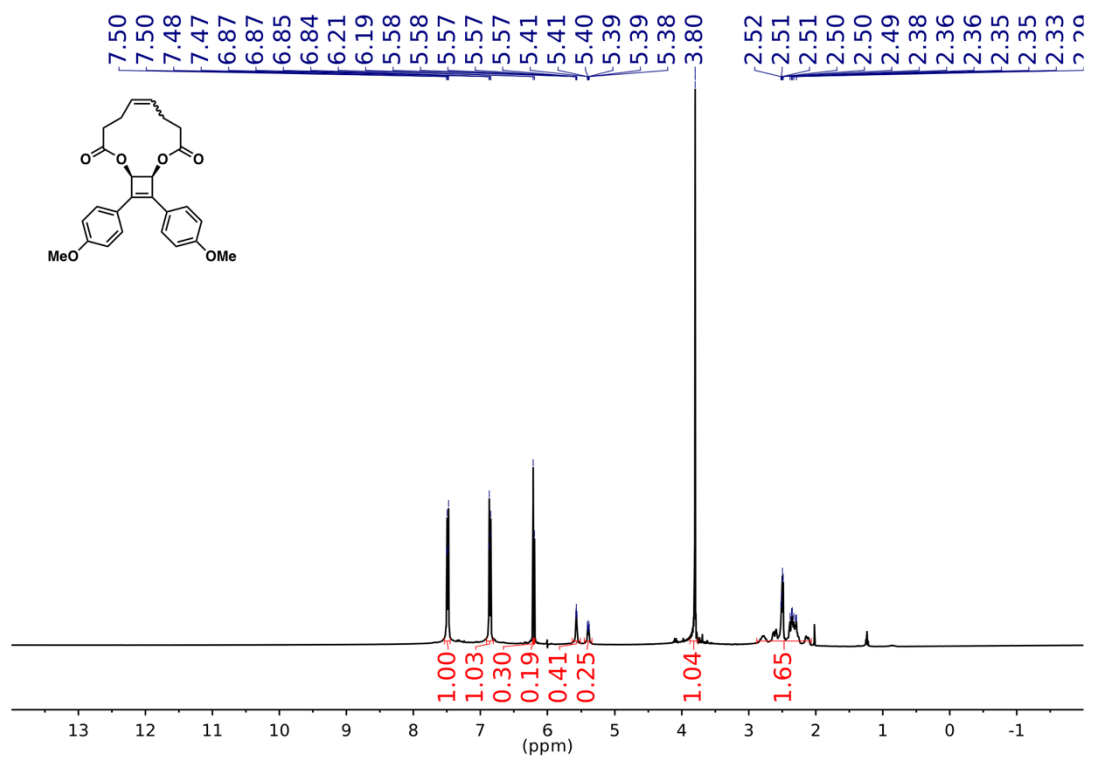
NMR Spectra of 1c-bisalkene



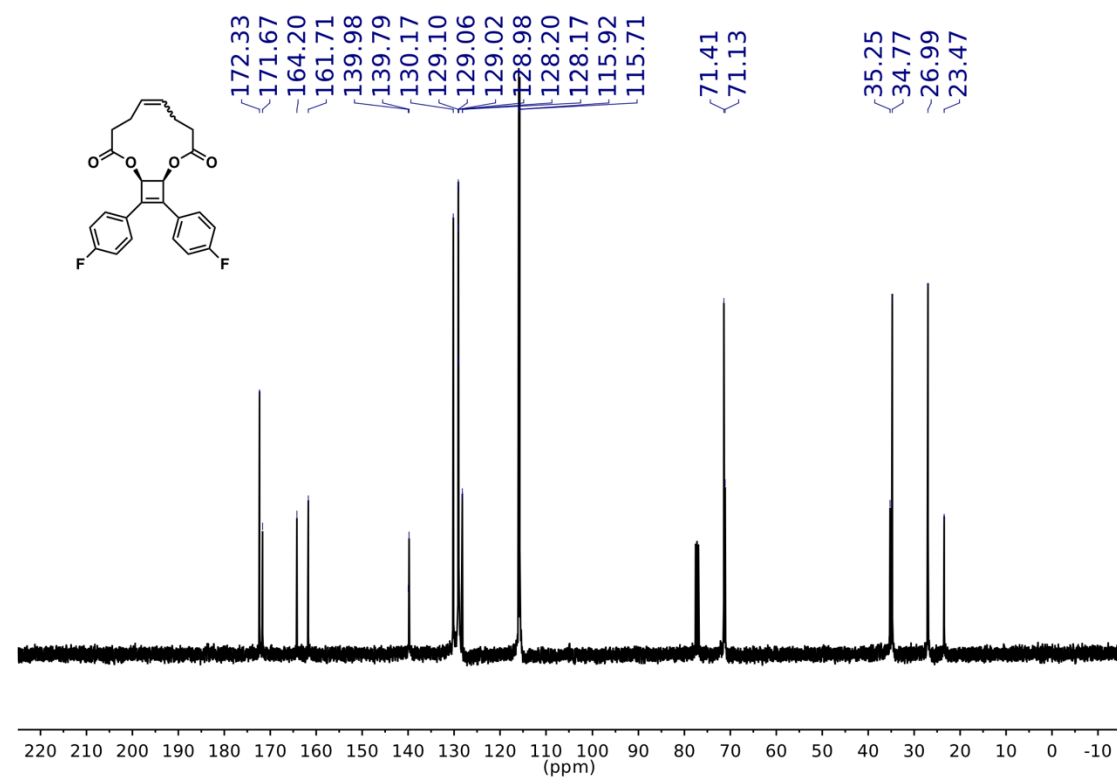
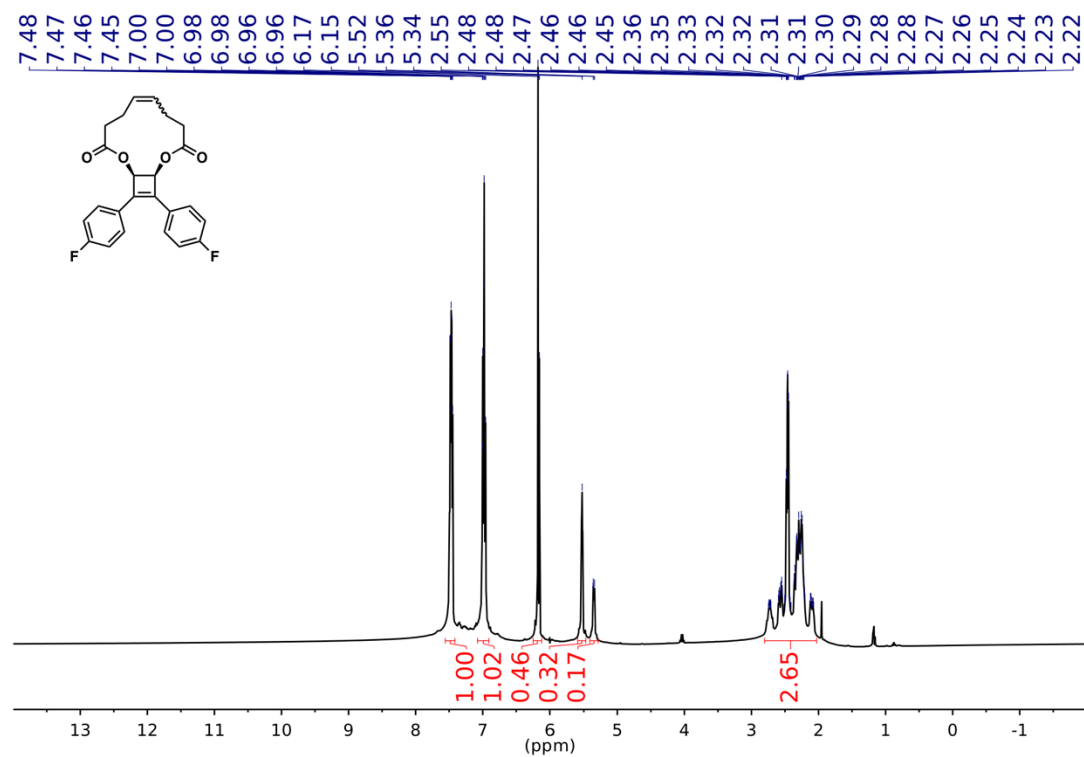
NMR Spectra of 2a-macrocycle



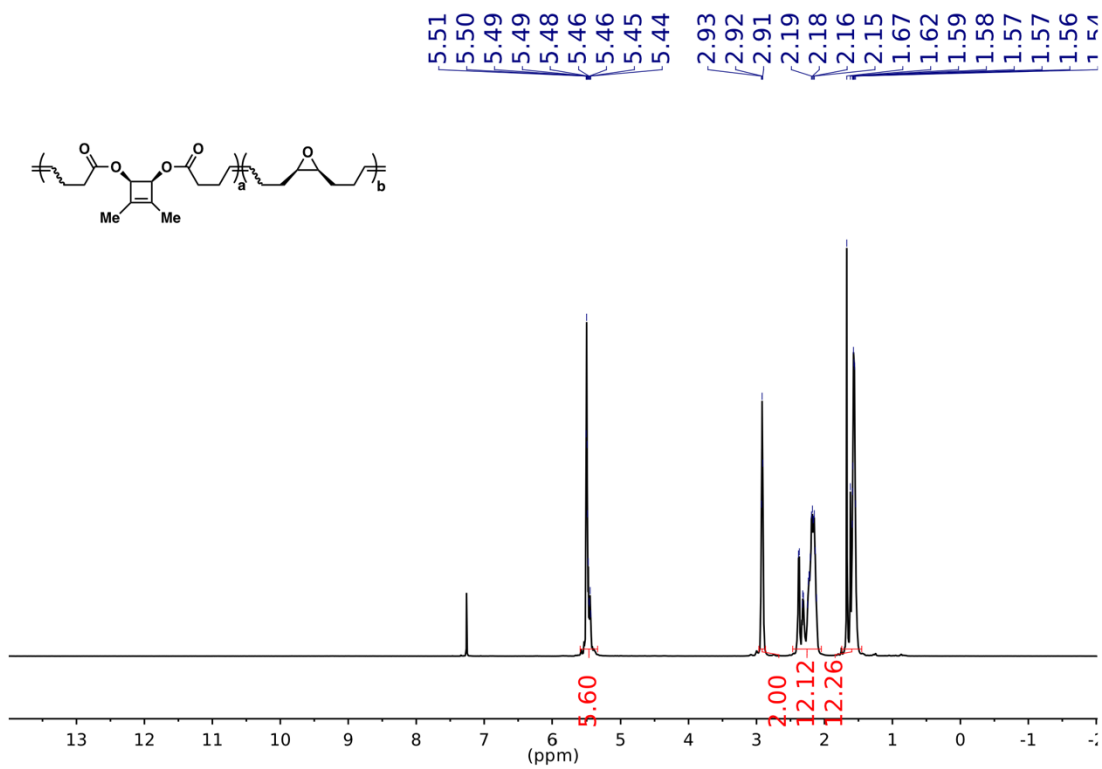
NMR Spectra of 1b-macrocycle



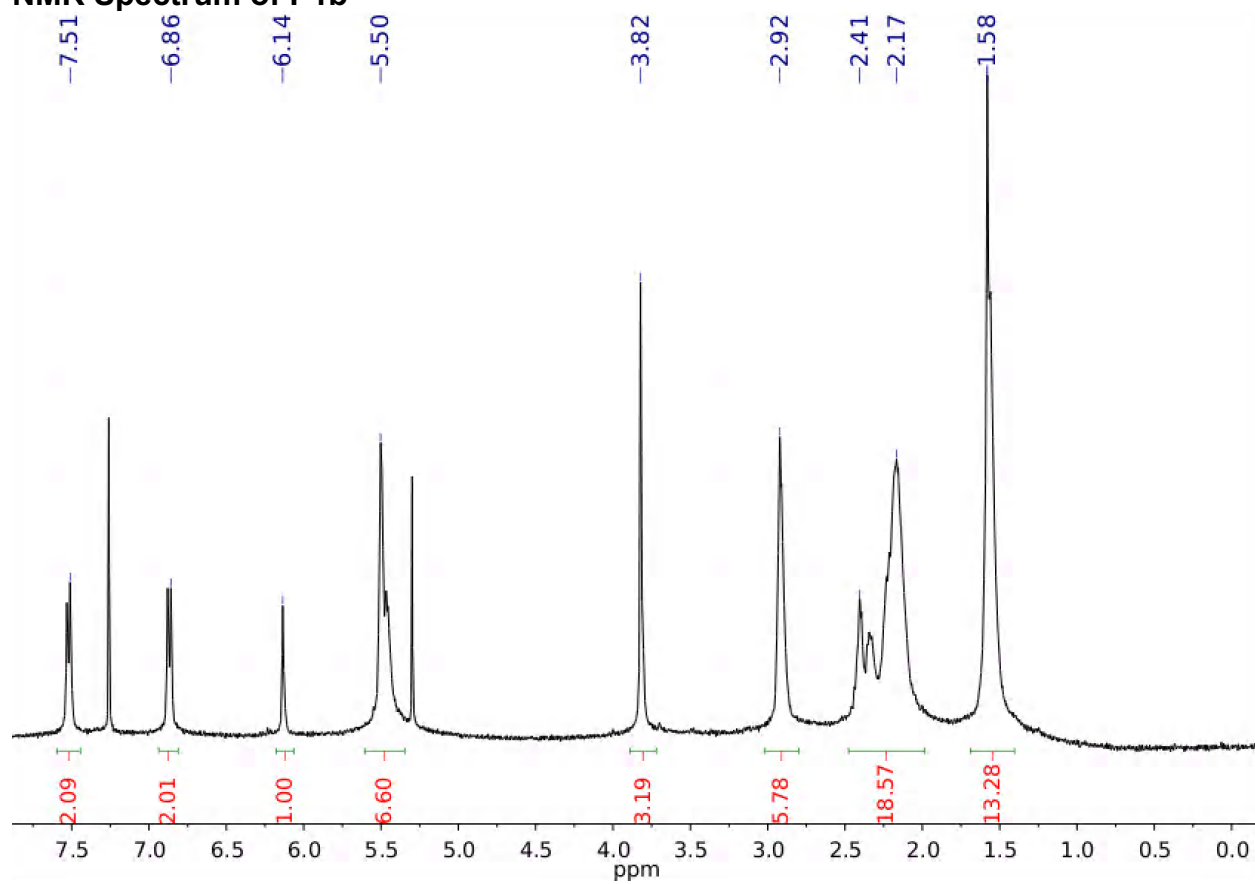
NMR Spectra of 1c-macrocycle



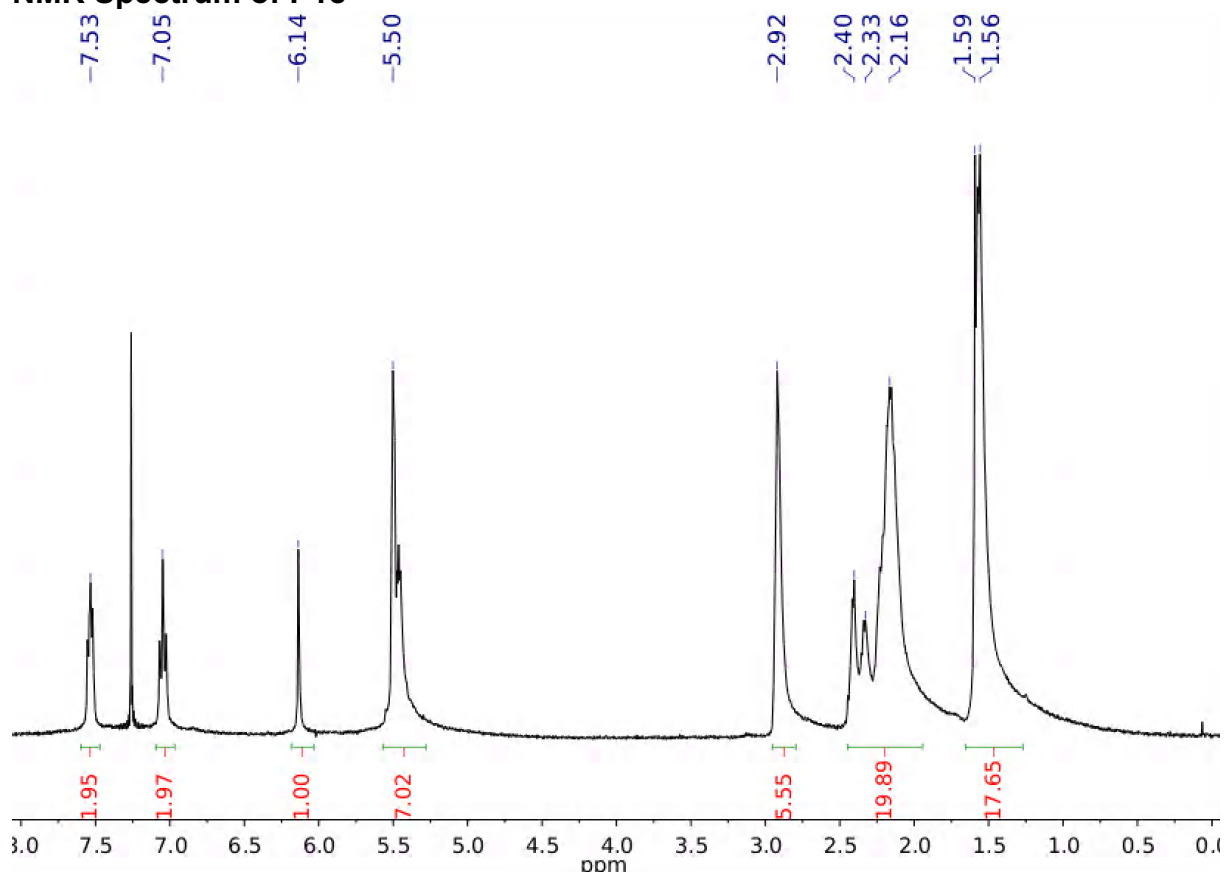
NMR Spectrum of P2a



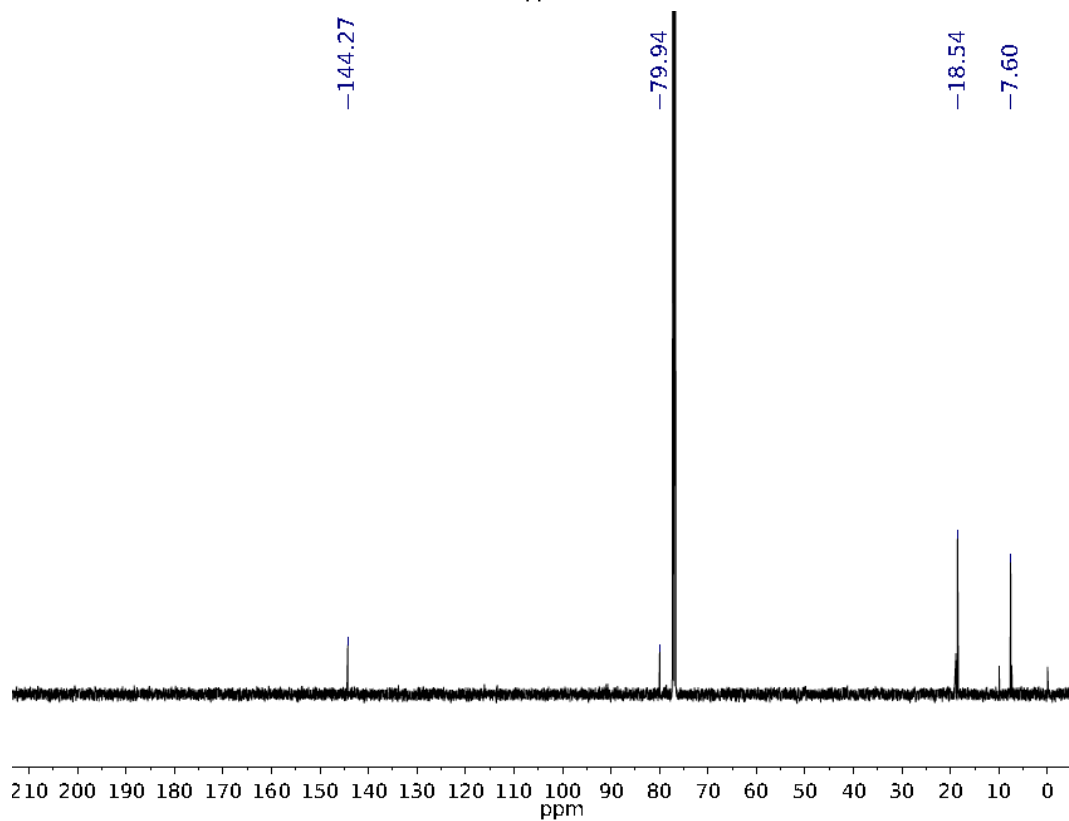
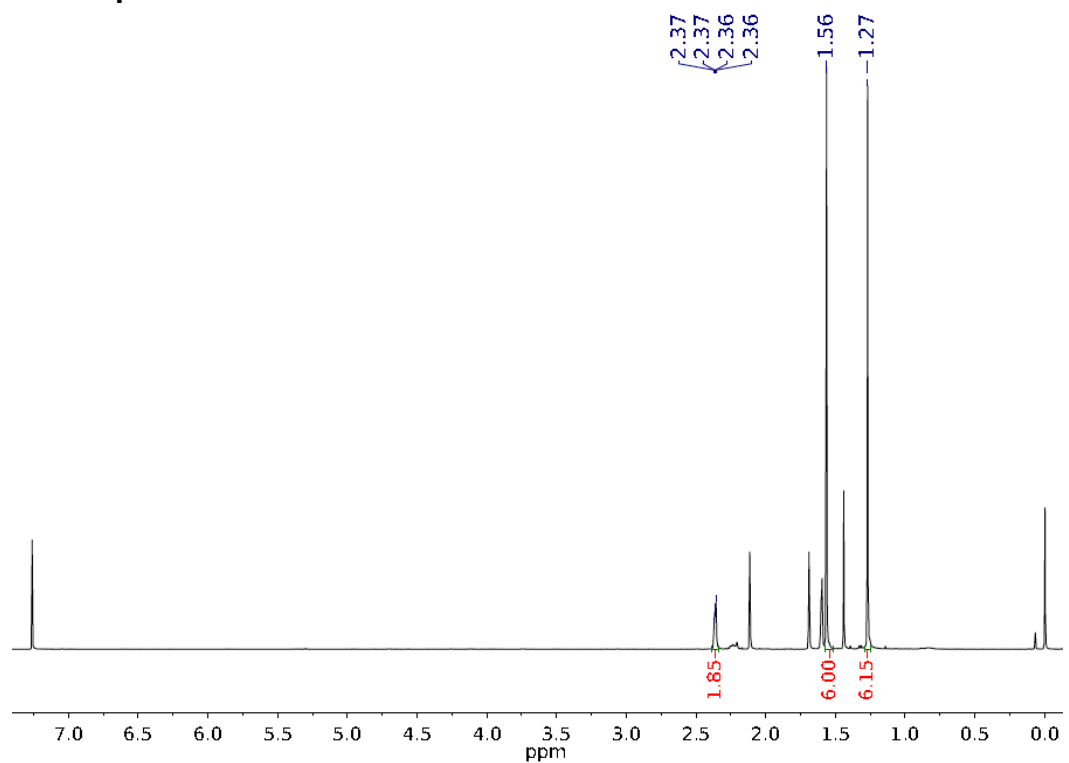
NMR Spectrum of P1b



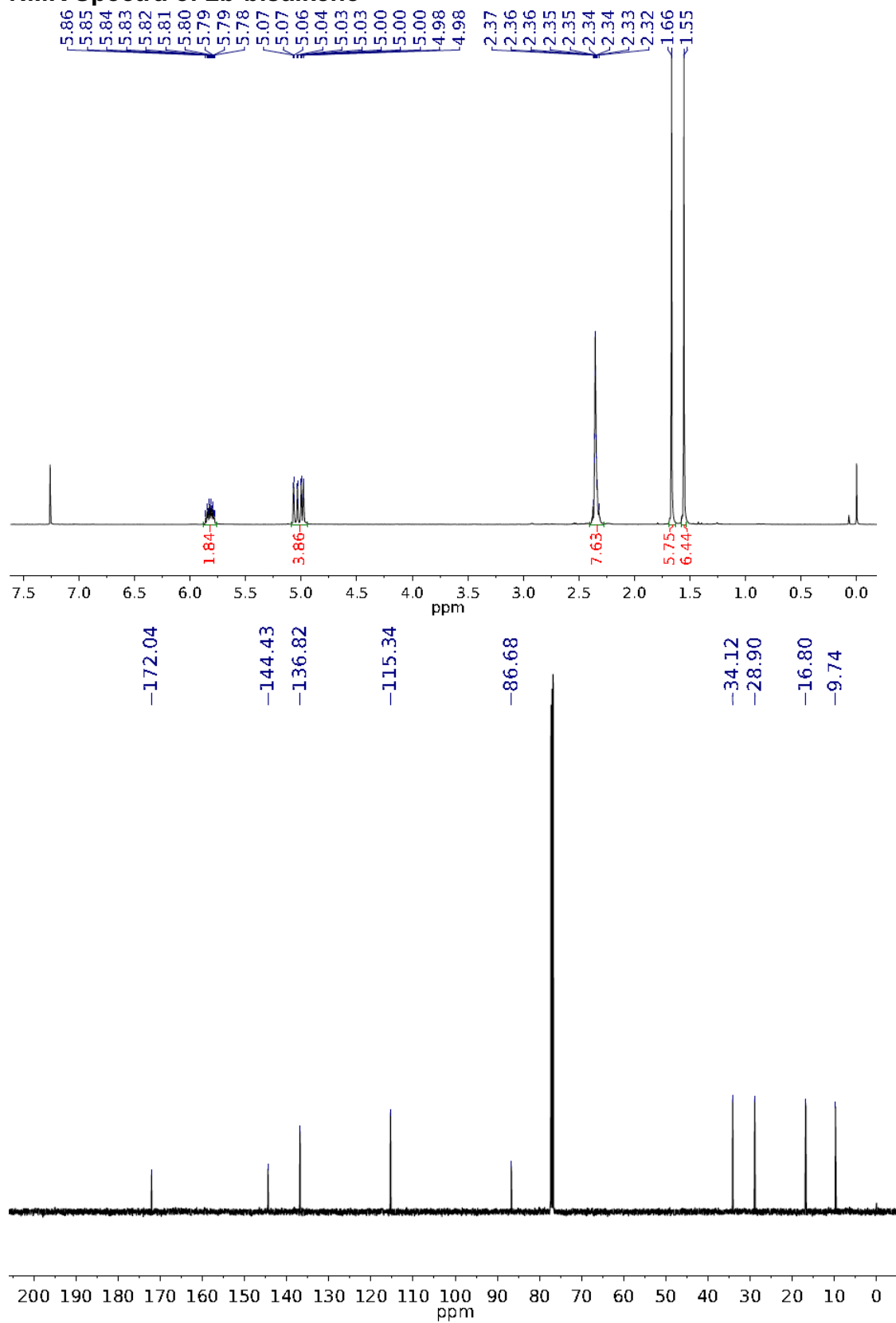
NMR Spectrum of P1c



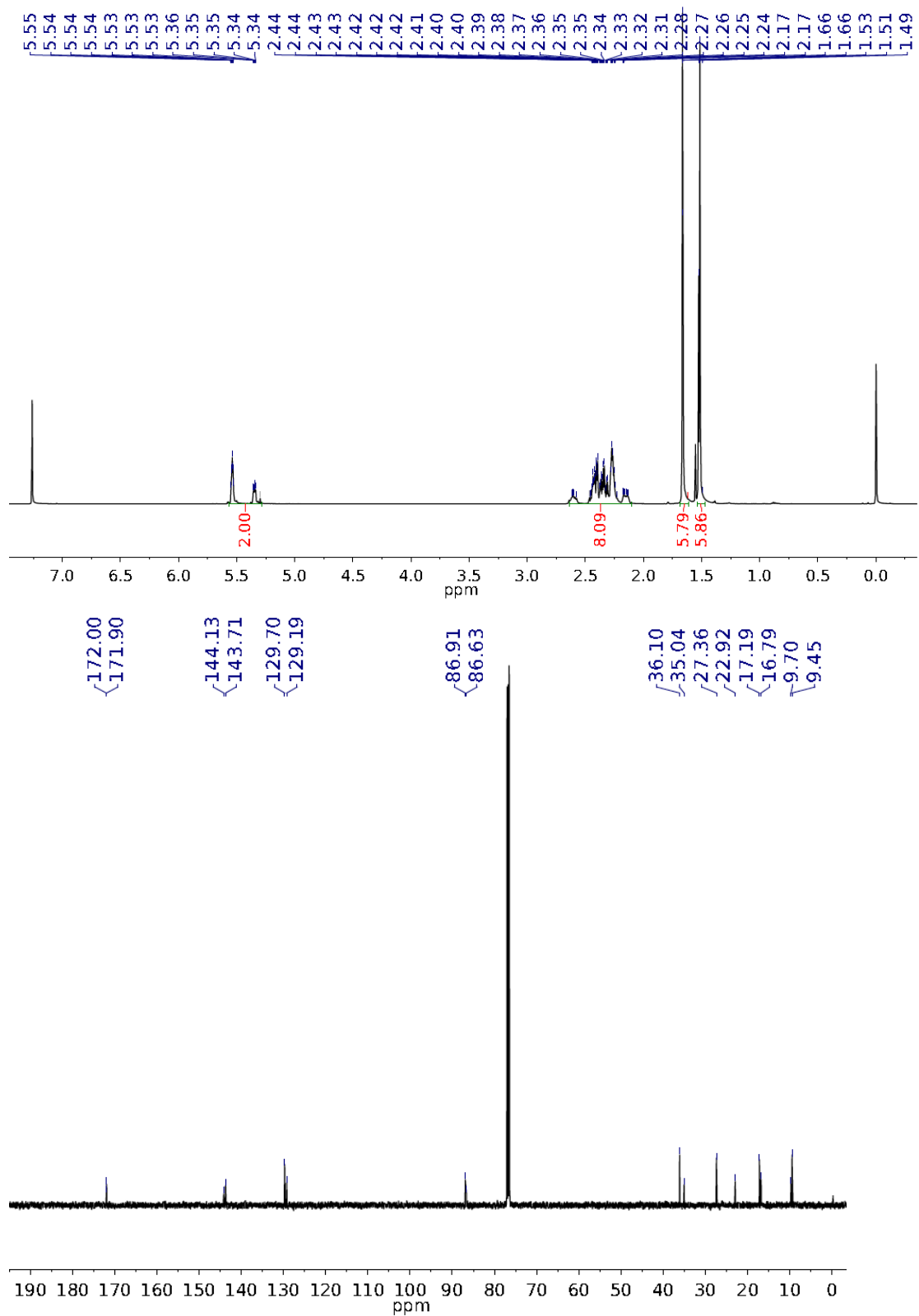
NMR Spectra of 2b-diol



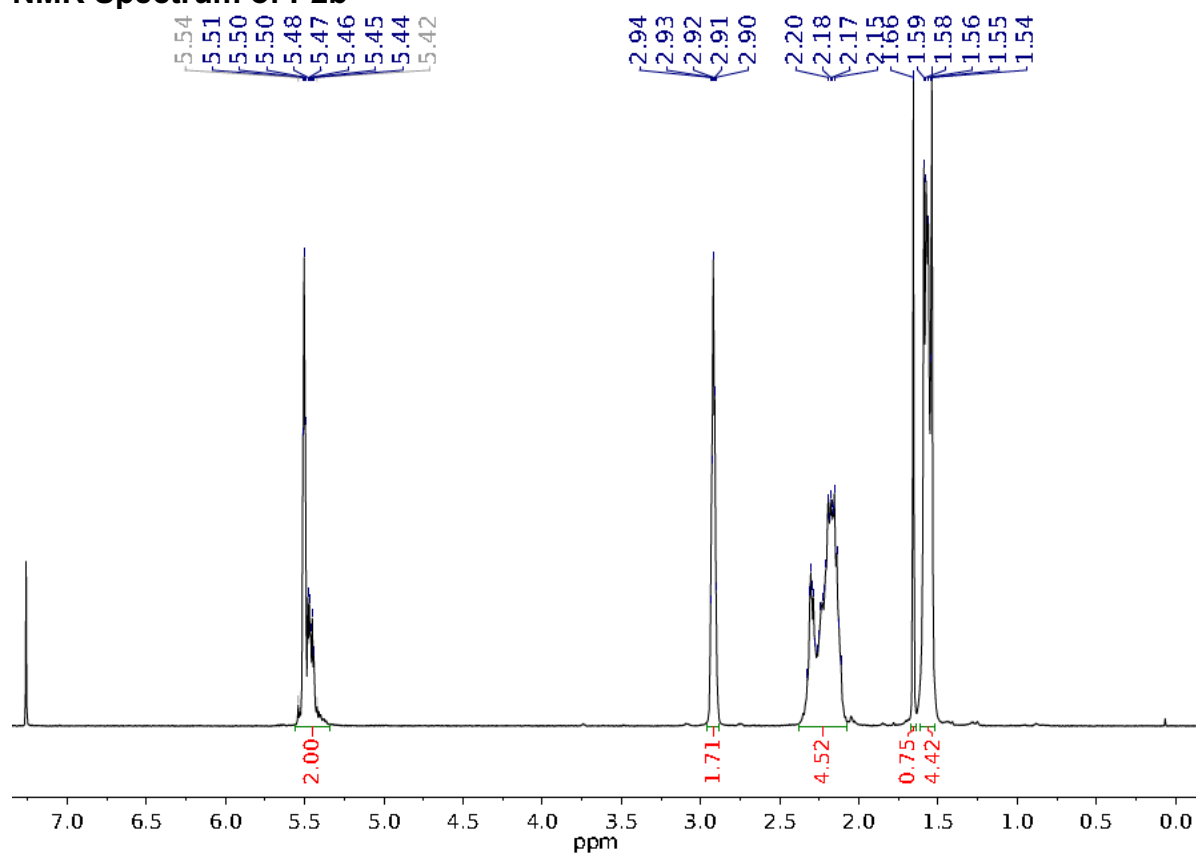
NMR Spectra of 2b-bisalkene



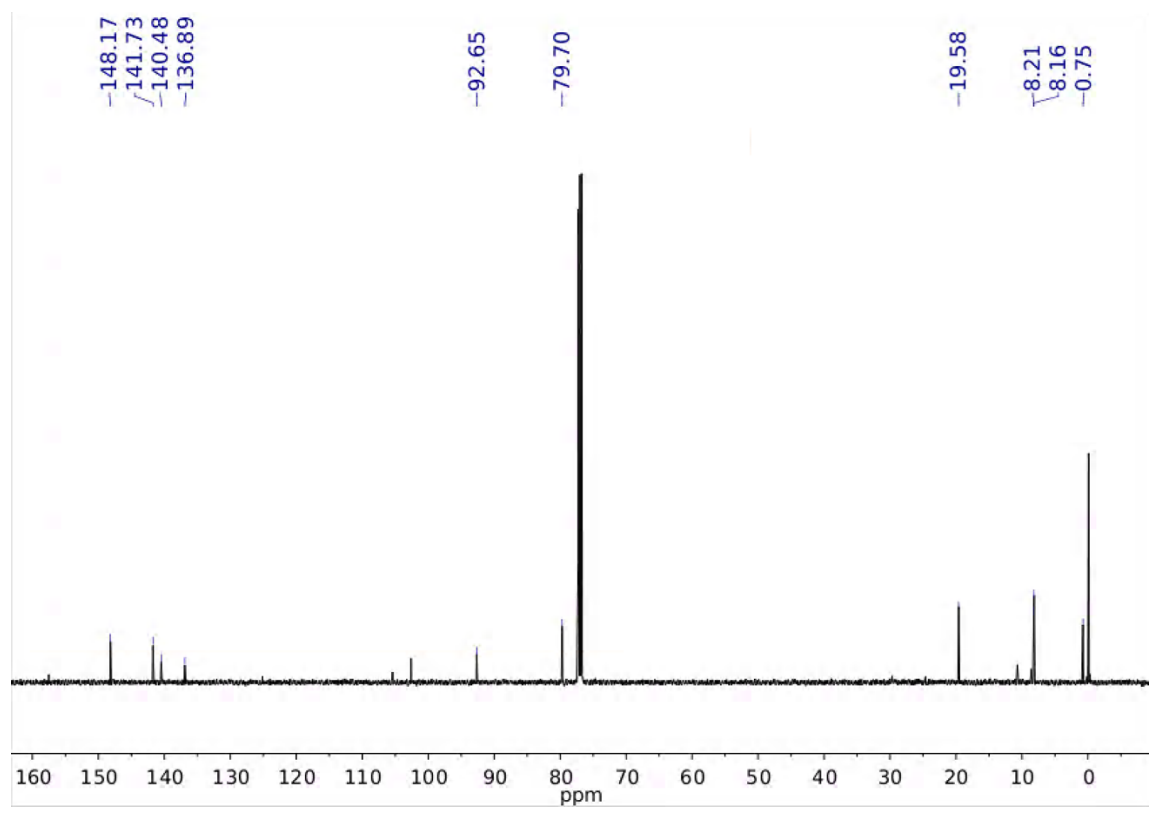
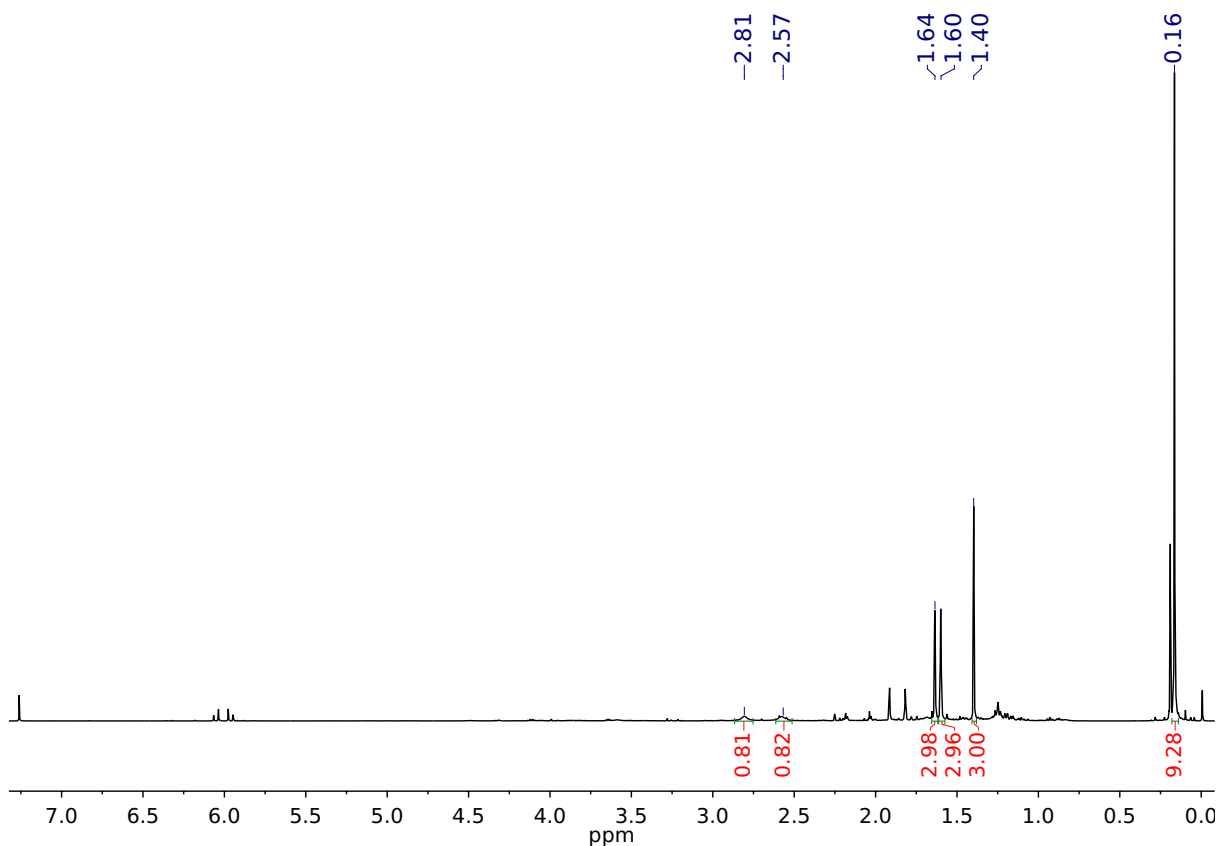
NMR Spectra of 2b-macrocycle



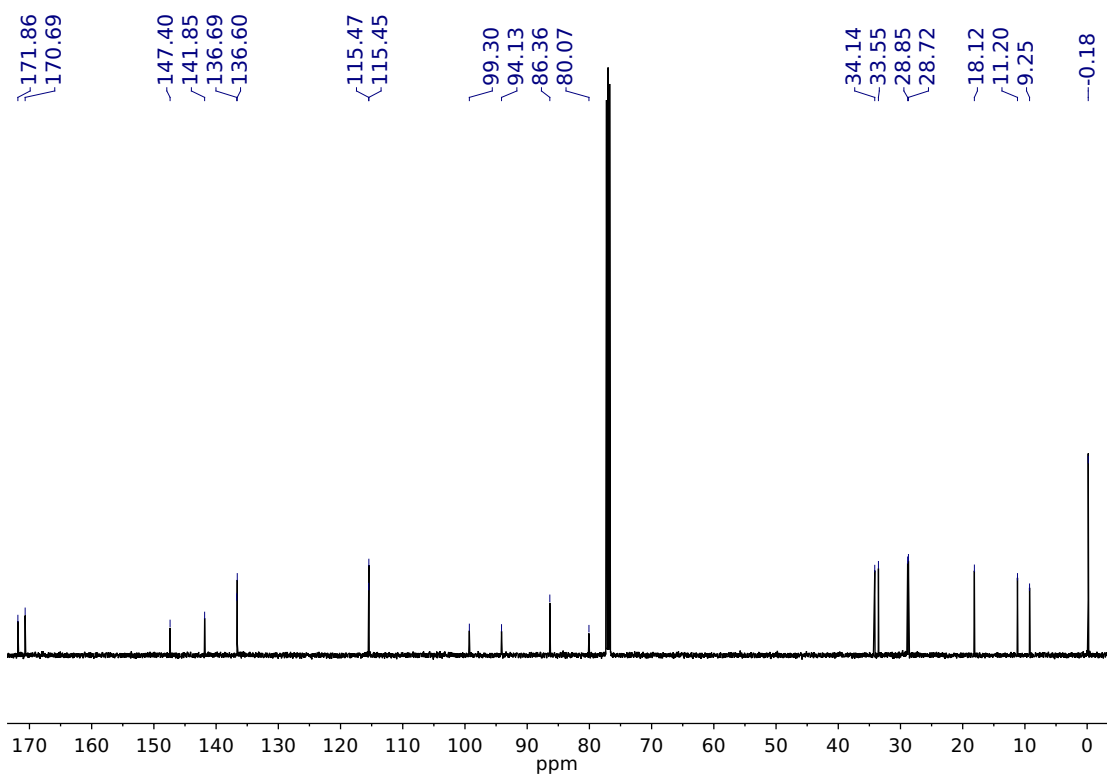
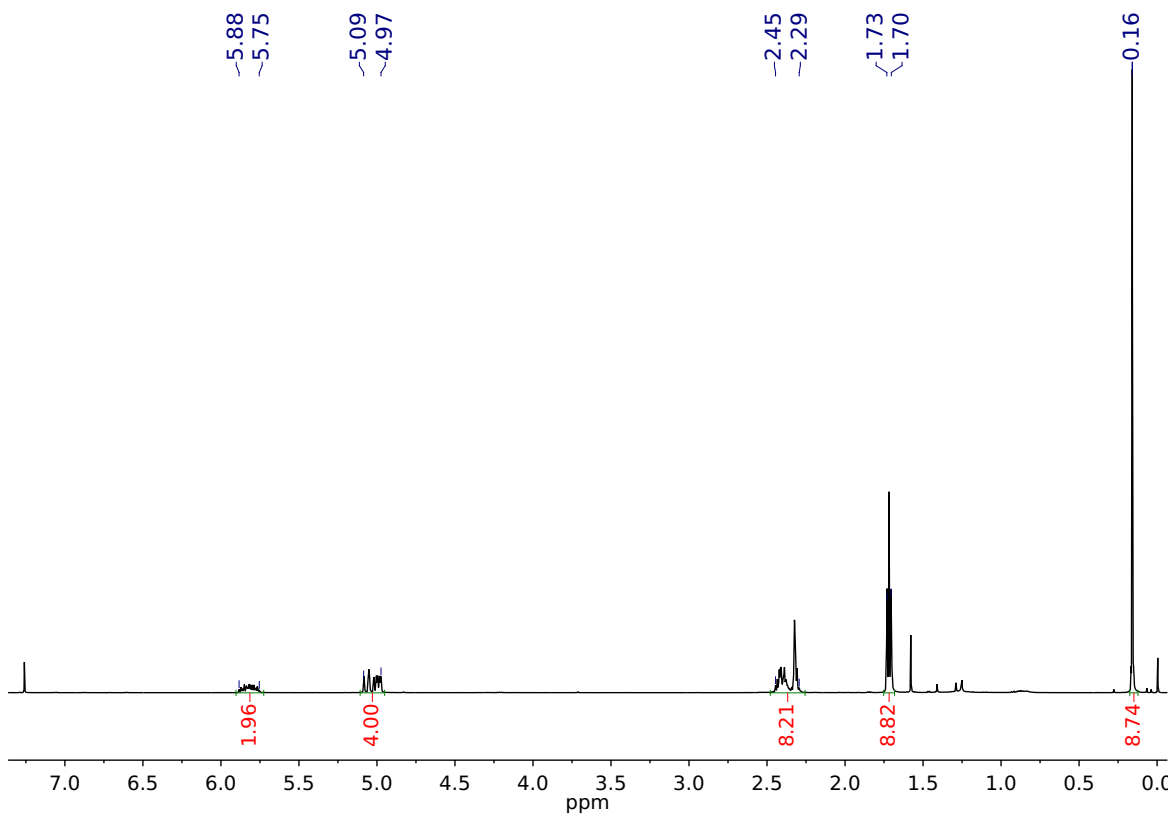
NMR Spectrum of P2b



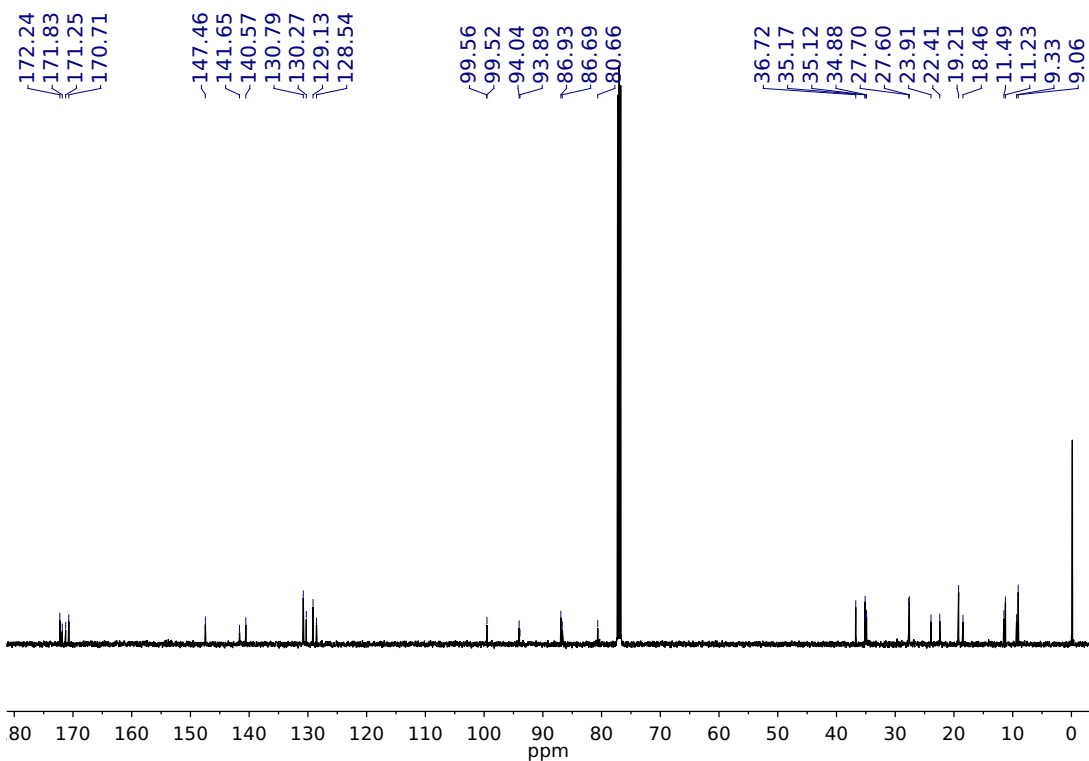
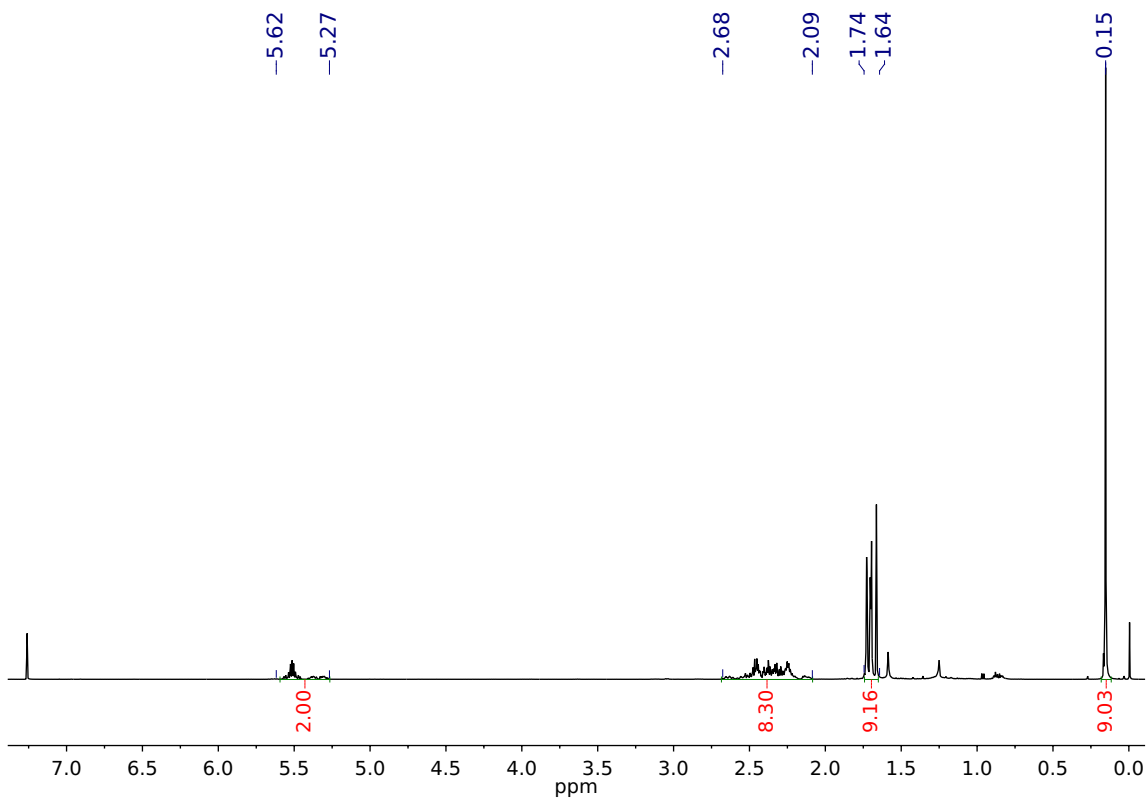
NMR Spectra of 2c-diol



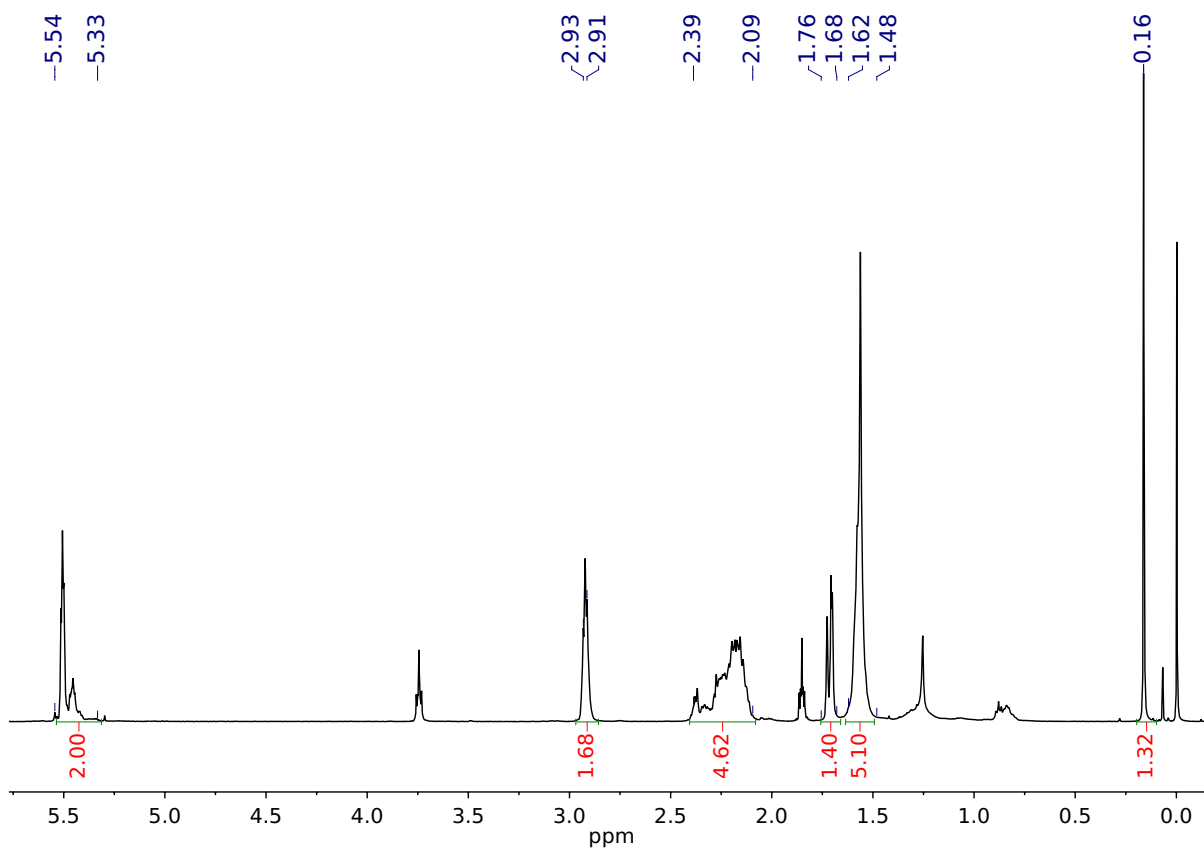
NMR Spectra of 2c-bisalkene



NMR Spectra of 2c-macrocycle



NMR Spectrum of P2c



References

1. Wu, D.; Lenhardt, J. M.; Black, A. L.; Akhremitchev, B. B.; Craig, S. L., Molecular Stress Relief through a Force-Induced Irreversible Extension in Polymer Contour Length. *J. Am. Chem. Soc.* **2010**, *132* (45), 15936-15938.
2. Klukovich, H. M.; Kouznetsova, T. B.; Kean, Z. S.; Lenhardt, J. M.; Craig, S. L., A backbone lever-arm effect enhances polymer mechanochemistry. *Nat. Chem.* **2013**, *5* (2), 110-114.
3. Wang, J.; Kouznetsova, T. B.; Niu, Z.; Ong, M. T.; Klukovich, H. M.; Rheingold, A. L.; Martinez, T. J.; Craig, S. L., Inducing and quantifying forbidden reactivity with single-molecule polymer mechanochemistry. *Nat. Chem.* **2015**, *7* (4), 323-327.
4. Wang, J.; Kouznetsova, T. B.; Niu, Z.; Rheingold, A. L.; Craig, S. L., Accelerating a Mechanically Driven anti-Woodward–Hoffmann Ring Opening with a Polymer Lever Arm Effect. *J. Org. Chem.* **2015**, *80* (23), 11895-11898.
5. Kouznetsova, T. B.; Wang, J.; Craig, S. L., Combined Constant-Force and Constant-Velocity Single-Molecule Force Spectroscopy of the Conrotatory Ring Opening Reaction of Benzocyclobutene. *ChemPhysChem* **2016**, n/a-n/a.
6. Oberhauser, A. F.; Marszalek, P. E.; Erickson, H. P.; Fernandez, J. M., The molecular elasticity of the extracellular matrix protein tenascin. *Nature* **1998**, *393* (6681), 181-185.
7. Florin, E. L.; Rief, M.; Lehmann, H.; Ludwig, M.; Dornmair, C.; Moy, V. T.; Gaub, H. E., Sensing specific molecular interactions with the atomic force microscope. *Biosens. Bioelectron.* **1995**, *10* (9), 895-901.
8. Adams, C. M.; Schemenaur, J. E.; Crawford, E. S.; Joslin, S. A., New Convenient Methods for the Preparation of Pendant Chain Cyclobutadiene Tricarbonyliron Complexes. *Synthetic Commun* **1992**, *22* (10), 1385-1396.
9. Liebeskind, L. S.; Fengl, R. W.; Wirtz, K. R.; Shawe, T. T., An improved method for the synthesis of substituted cyclobutenediones. *J. Org. Chem.* **1988**, *53* (11), 2482-2488.
10. Liu, Z.-y.; Wang, Y.-m.; Han, Y.-x.; Liu, L.; Jin, J.; Yi, H.; Li, Z.-r.; Jiang, J.-d.; Boykin, D. W., Synthesis and antitumor activity of novel 3,4-diaryl squaric acid analogs. *European Journal of Medicinal Chemistry* **2013**, *65*, 187-194.
11. Banert, K.; Grimme, S.; Herges, R.; Heß, K.; Köhler, F.; Mück-Lichtenfeld, C.; Würthwein, E.-U., Experimental and Theoretical Characterization of the Valence Isomerization of Bi-2H-azirin-2-yls to Diazabenzenes. *Chem. Eur. J.* **2006**, *12* (28), 7467-7481.
12. Höfle, G.; Steglich, W.; Vorbrüggen, H., 4-Dialkylaminopyridines as Highly Active Acylation Catalysts. [New synthetic method (25)]. *Angewandte Chemie International Edition in English* **1978**, *17* (8), 569-583.

13. Beyer, M. K., The mechanical strength of a covalent bond calculated by density functional theory. *J. Chem. Phys.* **2000**, *112* (17), 7307-7312.
14. Ong, M.T., et al., First principles dynamics and minimum energy pathways for mechanochemical ring opening of cyclobutene. *J. Am. Chem. Soc.* **2009**, *131* (18), 6377-6379.
15. Hariharan, P.C. and J.A. Pople, The influence of polarization functions on molecular orbital hydrogenation energies. *Theor. Chim. Acta.* **1973**, *28* (3), 213-222.
16. Becke, A.D., Density-functional thermochemistry. III. The role of exact exchange. *J. Chem. Phys.*, **1993**, *98* (7) 5648-5652.
17. Lee, C., W. Yang, and R.G. Parr, Development of the Colle-Salvetti correlation-energy formula into a functional of the electron density. *Phys. Rev. B*, **1988**, *37* (2) 785.
18. Vosko, S.H., L. Wilk, and M. Nusair, Accurate spin-dependent electron liquid correlation energies for local spin density calculations: a critical analysis. *Can. J. Phys.* **1980**, *58* (8) 1200-1211.
19. Stephens, P.J., et al., Ab initio calculation of vibrational absorption and circular dichroism spectra using density functional force fields. *J. Phys. Chem.* **1994**, *98* (45) 11623-11627.
20. Brown, C.L., et al., Substituent Effects in Mechanochemical Allowed and Forbidden Cyclobutene Ring-Opening Reactions. *J. Am. Chem. Soc.* **2021**, *143* (10) 3846-3855.
21. Seritan, S., et al., TeraChem: A graphical processing unit-accelerated electronic structure package for large-scale ab initio molecular dynamics. *Wiley Interdiscip. Rev. Comput. Mol. Sci.*, **2021** *11* (2) e1494.
22. Seritan, S., et al., TeraChem: Accelerating electronic structure and ab initio molecular dynamics with graphical processing units. *J. Chem. Phys.*, **2020**, *152* (22) 224110.
23. Kästner, J., et al., DL-FIND: an open-source geometry optimizer for atomistic simulations. *J. Phys. Chem. A*, **2009**, *113* (43) 11856-11865.
24. Metz, S., et al., Chem Shell—a modular software package for QM/MM simulations. *Wiley Interdiscip. Rev. Comput. Mol. Sci.*, **2014**, *4* (2) 101-110.
25. Sakai, S., Theoretical studies on the electrocyclic reaction mechanisms for s-cis butadiene and disilylbutadiene. *J. Mol. Struct.* **1999**, *461*, 283-295.